Vedecká rada Prírodovedeckej fakulty

Univerzity Pavla Jozefa Šafárika v Košiciach

Mgr. Petr Hanák

Mutational Analysis of UCP1 and Phylogenetic Relations within the Uncoupling Protein Subfamily

Košice, March 2004

Contents

1 Preface

Mitochondria are essential organelles involved in energy metabolism via oxidative phosphorylation. Besides their main metabolic functions, they play vital role in diverse biological processes such aging and apoptosis. In human, defects in the mitochondrial respiratory chain are responsible for or associated with a broad variety of diseases.
Practical outputs of study of mitochondria can lead, in the segment of research aimed to uncoupling of oxidative phosphorylation, to development of new drugs, effectively treating obesity, group of diseases in which reactive oxygen species play a important role, certain diseases of heart muscle, some neurodegenerative diseases, …

Uncoupling proteins are mitochondrial transporters of the inner mitochondrial membrane. According to general knowledge they are present in mammals; in plants they are represented by Plant Uncoupling Mitochondrial Protein(s). Here I report new members of the family from organisms such as *Dictyostelium discoideum*, *Caenorhabditis elegans* and *Drosophila melanogaster*.

To understand function of molecule of interest in depth (so that be able to modify it by various molecular interactions) one has to address the structure – function relationship. The study of functional importance of particular AA residues of rat UCP1 molecule constitutes ground of research in this dissertation.

In experimental part, methods of molecular biology were employed for construction of mutated forms of rat UCP1 and yeast biotechnology served as a tool for production of sufficient amount of the protein. Artificial proteoliposomes with incorporated particular mutant of UCP1 were prepared and transport characteristics of the protein were determined.

Interpretation of results of experimental part of this work is based on general assumption that when certain aminoacid residue plays critical role for the function, then its impairment must knock out this function in proportional extent and vice versa.

In another part of this work homology between known and newly found (by means of BLAST search in genome and protein databases) uncoupling protein candidates was assessed. Besides classical comparisons of percent of homology, which enabled construction of phylogenetic trees,

less "normalized" but more concise comparison of previously proposed functional sequences was accomplished. Both approaches came to more or less same conclusions.

2 Introduction

2.1 Thermogenesis (on the organismal and cellular level)

The tissue most specialized for thermogenesis in mammals is brown fat, abbreviated as BAT (from Brown Adipose Tissue). In some species (rodents) BAT is present during all lifetime, its development or mass can be induced by exposure to cold. In large mammals, including human, the BAT is well developed throughout their neonatal life. In rodents (represented by rat or hamster), BAT is the main source of nonshivering thermogenesis. The relative thermogenic performance (when the same mass of tissue is considered) of BAT is 60 fold higher than the efficiency of liver.

The main control system of BAT activity is located in hypothalamus and acts through thermoregulatory centers and sympathetic nerves that innervate the brown adipocytes directly [1].

BAT is found in characteristic deposits scattered in specific areas in the body, the major deposits being interscapular, axillar, perirenal, thoracic and between the neck muscles. When BAT starts producing heat, this is quickly cleared through large vessels that convey it to the thoracic spinal chord, heart, thoracic structures, brain and kidneys [1].

The brown color of BAT is due to the high density of mitochondria, compared to white adipose tissue. Organismal control of BAT is based mainly on sympathetic innervation. BAT is densely innervated by sympathicus. Terminal ends of SNS (sympathetic nervous system) release hormone norepinephrine. NE´s thermogenic action is pleiotropic: NE stimulates differentiation of preadipocytes into BAT cells as well as growth of BAT. It also increases a number of mitochondria in BAT cells [2]. Norepinephrine stimulates β-3 adrenergic receptors on plasmatic membrane of brown adipocytes. β-receptor is connected to stimulatory G-protein. Adenylate cyclase is the next element of this signal transduction pathway, producing cyclic AMP (cAMP). cAMP represents a second messenger, which stimulates protein kinase A. Protein kinase A has two main targets: Hormone-sensitive lipase serves as one of them. Once phosphorylated lipase breaks down triacylglycerol. Macroscopic manifestation of this is hydrolysis of multilocular triglyceride droplets in brown adipocytes. One of the products of this reaction, free fatty acids,

directly interacts with UCP1 molecules and stimulates uncoupling. Another target of protein kinase A is the cAMP-response-element-binding-protein (abbreviated as CREB). Via CREB the transcription of UCP1 gene is stimulated in nucleus, hence the uncoupling potential in mitochondria is eventually increased [3,4]. Fig. 1.

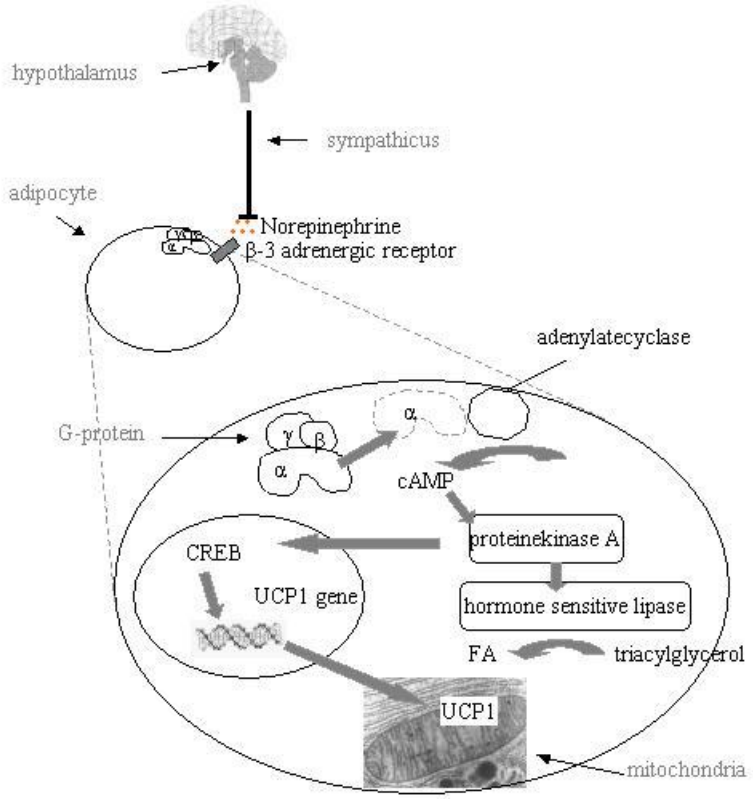

Fig. 1: Simplified scheme of the main regulatory mechanism controlling heat production by brown fat tissue.

Besides this main signal transduction pathway several other pathways and regulatory steps exist: α-1, β-1 and β-2 adrenergic receptors are involved in some extent. Stabilization of UCP1 mRNA is affected, hence increase of effectiveness of the relation between gene stimulation and protein production, is one of effects of norephinephrine.
NE also stimulates thyroxine deiodinase activity. Triiodothyronine (abbreviated as T_3) is produced. T_3 stimulates transcription of UCP1 gene [5,6].
Another stimulator of UCP1 gene transcription is retionic acid [3].
Insulin like growth factor (IGF-I) seems to play role in regulation of UCP1 expression via increase of CCAAT/enhancer binding protein α (C/EBPα) and decrease of CCAAT/enhancer binding protein δ (C/EBPδ) levels. These transcription factors bind to response elements in enhancer sequence of UCP1 gene [7,8].

In this context it is necessary to mention the influence of pH on binding of inhibitory nucleotides, thus uncoupling mitochondria upon alkalization. Despite of clear dependence of this process on pH in experiments in vitro, exploitation of this mechanism in physiological conditions is in doubt [9].

In one report, mitochondria carrying UCP1, so that capable of controlled heat production, are reported in mammals living in constantly cold conditions also in other tissues than BAT.

Uncoupling (represented by increased substrate oxidation and heat production) is observed when the BAT UCP1 is working in a) animals exposed to the cold b) when hibernators are waking from hibernation c) in newborn mammals [1].

Rapid and prolonged increase in the level of uncoupling protein mRNA is observed in rats after exposure to cold, at birth, etc. β-adrenoreceptor agonist BRL 26830A functions in the same stimulatory way. The acute transcriptional response starts 15 minutes after beginning of stimulation [10].

UCP-deficient mice consume less oxygen after treatment with a $beta_3$-adrenergic-receptor agonist and they are sensitive to cold, indicating that their thermoregulation is defective. On the other

hand no obesity is caused by this defect in mice fed on either a standard or a high-fat diet. This could be due to compensation of UCP1 impairment by UCP2 [11].

Transgenic mice expressing UCP1 constitutively also in white fat (2 – 10% of the BAT expression) display reduced mass of subcutaneous fat. In genetically obese mice strain Avy constitutive expression of UCP1 leads to decrease of total body weight to the normal "non-obese" level as well as to reduction of subcutaneous fat [12].

2.2 Mitochondria

2.2.1 Electrochemical gradient

Oxidative phosphorylation., i.e. production of ATP molecules, represents one of the most critical functions of mitochondria. This endergonic process of ATP synthesis from ADP and P_i is catalyzed by enzyme ATP-ase (complex V). Production of ATP is coupled to translocation of protons from intermembrane space back into the mitochondrial matrix. Free energy for this synthesis is obtained from proton electrochemical gradient μ_{H+}, created by the process of electron transport that runs in the cascade of enzyme complexes of the respiratory chain, integrated into inner mitochondrial membrane:

EQ. 1
$$\Delta\tilde{\mu}_{H+} = \Delta\Psi - \frac{2.3RT}{F}\Delta pH$$

In normal situation, the electron transport is tightly coupled with the oxidative phosphorylation because the electrochemical gradient prevents further proton pumping and so inhibits electron transport. There are compounds allowing protons to get back to matrix and dissipate the proton electrochemical potential. The result is the fall of μ_{H+} and the production of heat. There exist synthetic uncouplers (dinitrophenol, FCCP, CCCP) as well as natural ones - uncoupling proteins.

It was proposed that an increased proton permeability of the mitochondrial inner membrane, not coupled to an energy-consuming system such as ATP synthase, would constitute a proton leak

and decrease the level of coupling of respiration to ATP phosphorylation. Mild constant uncoupling of respiration could also function in preventing of accumulation of oxygen radicals generated by mitochondria or in increasing sensitivity and rate of oxidative phosphorylation to effectors as well as in control of NAD^+/NADH ratio [1,13].

The respiratory states of mitochondria are classified into 5 grades:

State 1: Respiration is low, because of lack of substrate and ADP
State 2: Respiration is low, because of lack of substrate; ADP is present
State 3: Respiration is high, since there is enough of substrate and ADP
State 4: Respiration is low, because ADP is exhausted
State 5: Respiration is low, because oxygen is exhausted

The respiration required to maintain the protonmotive force against the proton leak is represented by the state 4 respiration rate in mitochondria.

2.2.2 BAT mitochondria

BAT mitochondria differ from another types of mitochondria in their relative permeability for chloride and bromide anions at neutral pH. This observation was one of the historical building blocks of the mosaic finished by discovery and characterization of UCP1. Another observation shows that in the absence of albumin (which eliminates fatty acids) there is no difference in rates of swelling between H^+ uniport initiated by ionophore valinomycin and H^+/K^+ antiport. Effect of ionophore nigericin was the first indication that brown adipose tissue mitochondria could be permeable for protons [4].

A specific binding site for purine nucleotide was determined on the outher surface of the inner membrane of brown adipose tissue mitochondria [14,15]. The number of these binding sites was found to increase during cold adaptation, corresponding to to the thermogenic activity of brown adipose tissue [14].
Indirect evidence of brown fat mitochondria specialization for thermogenesis is the relatively low content of ADP/ATP carrier when compared to the beef heart mitochondria. This fact documents

that the production of energetic metabolites in BAT mitochondria is suppressed and replaced by heat production as the main function [16].

At the temperature 25 ^{o}C and physiological levels of the membrane potential, the molecular activity of UCP1 does not exceed 5000 min^{-1}. In hamster brown adipocytes there are two to four UCP1 molecules per one molecule of cytochrome oxidase [17].

2.3 Mitochondrial anion carrier proteins

2.3.1 Family of mitochondrial carrier proteins

Mitochondrial carrier proteins seem to have evolved by diversification from a common gene coding for a domain of about 100 residues [17]. Typical representatives of this family are, excluding UCP subfamily, ADP/ATP carrier, phosphate carrier, dicarboxylate carrier, oxoglutarate malate carrier, Graves´ disease carrier [1,18].

Two members of this family – phosphate carrier and ADP/ATP carrier emerged in evolution at the moment of endosymbiotic origin of mitochondria, hence they are not present earlier then in eucaroytes. This is in contrast to other protein components of oxidative machinery such as cytochromes or ATP synthase which have their prokaryotic ancestors [17].

2.3.2 Phylogenetical relations in MACP family

Originally ADP/ATP carrier was considered to be the closest relative of UCPs. Its molecular weight is nearly identical to the molecular weight of UCP1. Also the feature of binding nucleotides is common to members of both of these groups. The unique isolation procedure is (except steps for separation of UCP1 from ADP/ATP carrier) also the same: exclusion from hydroxylapatite in nonionic detergents. Both form a dimer with only one binding site for nucleotides.

Tripartite structure is another feature linking UCP family to another members of MACP family. This feature is also typical for ADP/ATP carrier as well as for phosphate carrier. There are common motifs which exist throughout all domains of these three groups within MACP family [17].

On the other hand, phylogenetic trees based on homology show that oxoglutarate-malate carrier is the closest relative of UCPs within the whole family (Hanák, Ježek – unpublished results) [19].

Analysis of several genomic clones encompassing UCP2 and/or UCP3 genes demonstrated that these genes are adjacent, the human UCP2 gene being located 7 kb downstream of the UCP3 gene [20]. Closeness of these two genes (in mouse on chromosome 7, in human on chromosome 11) indicates that they originated by duplication of one gene [1].

Two novel UCP molecules were detected recently when cross-reacting anti-PUMP antibody was employed:

UCP (m.w. 32 000) was detected in mitochondria of protozoan - nonphotosynthetic soil amoeboid *Acanthamoeba castellani.* Another UCP was found in fungi mitochondria – in yeast *Candida parapsilosis*. Physiological characteristics of these UCPs correspond in the best way to PUMP – stimulation by fatty acids and relatively weak inhibition by purine nucleotides.

The discovery of these UCPs are presented as indicative of UCPs origin, as specialized proteins for H^+ cycling, early during phylogenesis before the major radiation of phenotypic diversity in eucaryotes [21,22].

2.3.3 Sequential topology of UCP subfamily

Comparison of AA sequences of known UCPs led to finding of conserved sequences, unique just for UCPs, so that segregating them from other members of MACP family. Assumption was made, that when particular sequence is common for UCPs and is not present in other MACPs, there is high probability that this sequence could be involved in UCP function (i.e. H^+ uniport induced by fatty acids, transport of various anions and inhibition of this transport by purine nucleotides).

Second matrix segment signature is conserved in rigorous way in all UCPs except BMCP/UCP5. It starts with Arg 152 and the sequence can be expressed by formula [+]- ϕ-X-Gly/Ser-Thr/n-X-NH/[-]-Ala-ϕ . In this formula [+] stands for residue with positive charge, [-] stands for residue with negative charge, ϕ stands for aromatic residue, n stands for nonpolar residue, NH stands for Asn or His, X stands for any residue.

First transmembrane α–helix is characterized by characteristic sequence formula Ala/Ser-Cys/Thr/n-n/Phe-Ala/Gly-[-]-n/F-n/Cys-Thr-Phe/n. This UCP signature is delineated by Ala23 in direction $NH_3^+ \rightarrow COO^-$ end. In modified form this conserved sequence applies also to BMCP/UCP5.

The sequence Gly/Ala-Ile/Leu-Gln/X-[+]-NH-n/Cys-Ser/n-ϕ/X-n/Ser-OH/Gly-n-[+]-Ile/Met-Gly/Val-n/Thr is characteristic for second transmembrane α–helix. Its motif starts at the position 80 of UCP1.

The fourth transmembrane α–helix spans area that is believed to be the core part of purine nucleotide binding domain. The general formula is: Pro-Asn/Thr-n-X-[+]-Asn/Ser/Ala-n-Ile/Leu-n-Asn/Val-Cys/n-n/Thr-[-]-n-n/Thr/ Pro-OH/Val. First proline of this UCP signature is at the position 178 [23].

2.3.4 Uncoupling proteins

2.3.4.1 UCP2

UCP2 is 59% homologous to UCP1 and 73% homologous to UCP3. Gene for UCP2 is localized on chromosome 7 in mouse and on chromosome 11 in human. At the time of first cDNA clonings, UCP2 was referred as UCP homolog (UCPH). Gene for UCP2 is composed of 8 exons. Two of them – exon I and II are not translated. Remaining six exons form couples. Each couple corresponds to one domain of tripartite structure of UCP2 molecule [20]. Expression of UCP2 gene is much broader than the expression of UCP1. Predominantly UCP2 is expressed in white adipose

tissue, in skeletal muscles and also in tissues rich in macrophages (spleen, thymus, bone marrow, intestine etc.) and in lung. Expression is cold inducible – 48 h cold exposure increased UCP2 mRNA in BAT, heart and soleus muscle. On the contrary fasting had no effect on UCP2 mRNA expression either in BAT or in heart, but markedly increased it in skeletal muscles [24].

In white fat UCP2 is upregulated upon fat feeding. Adipocyte hormon leptin upregulates UCP2 in tissues expressing the leptin receptor OB-R [25]. In adipose tissue of ob/ob and db/db mice, the UCP2 transcript is induced approximately fivefold relative to lean littermate controls. Flow cytometric experiments done with potential sensitive dye indicate decrease in the mitochondrial membrane potential in yeast in which murine UCP2 was expressed. When the distribution of populations is compared between UCP1 and UCP2, extra peak, corresponding to higher uncoupling in UCP2 mitochondria than in UCP1, can be seen. Hence, more potent uncoupling effect of UCP2 than UCP1 can be expected. This expression also resulted in growth inhibition under conditions that require aerobic respiration, but does not affect growth under anaerobic conditions [1,26-28].

UCP2 expressed in *Escherichia coli* and then reconstituted into proteoliposomes catalyzes electrophoretic flux of protons and alkylsulfonates. Fatty acids act in the same stimulatory way as in case of UCP1. Purine nucleotide inhibition was observed but with weaker response to the inhibitor. Hence uncoupling function in cells is supposed. [29].

Fleury et. al hypothesize, that UCP2 can be key factor in thermogenic responses to inflammatory stimuli [27]. Detection of high-level expression of UCP2 in hepatic Kupffer cells by cross-reacting antibody against UCP1 [30] seems to support this hypothesis.
Expression of UCP2 mRNA in monocyte/macrophage cells is in fetal liver 30-fold higher than in cells of adult animals. This indicates involvement of UCP2 in development of haematopoetic system [31].

2.3.4.2 UCP3

UCP3 is 57% homologous to UCP1 and 72% homologous to UCP2. Gene for UCP3 is composed of one untranslated exon and six (II - VII) exons coding protein molecule. Human UCP3 mRNA exists in short and long forms [1].
UCP3 is expressed predominantly in skeletal muscle and BAT. Expression of this gene is not affected by exposition to cold, but the level of UCP3 mRNA is influenced by hormonal and

dietary manipulations – fasting increases its level in muscle. Generally its role in energy balance and lipid metabolism is referred [28,32,33].

Experiments were done on transgenic mice carrying (extra) gene for human UCP3, controlled by α-skeletal actin promoter. Expression of UCP mRNA was increased in muscles 66-fold. The main phenotypic manifestation of increased UCP3 expression is reduction of weight. Also increased muscle temperature was observed, however the whole body temperature was unaffected. These results are in agreement with hypothesized involvement of UCP3 in lipid substrate utilization as its main or ultimate function [34].

In skeletal muscle, UCP3 expression did not change in response to 48 h of cold exposure, whereas it is generally increased up to 5.6-fold levels after food restriction or fasting. In soleus muscle of obese (fa/fa) rats UCP3 expression is decreased by 36% when compared with lean Zucker rats. These findings provide ground for hypothesis that UCP3 is regulated in a way to "counterbalance" drops of heat production of BAT, so that the total body heat production is maintained within certain limits [35].

Also muscle UCP3 levels were decreased 3-fold in hypothyroid rats and increased 6-fold in hyperthyroid rats. White adipose UCP3 levels were greatly increased by treatment with the β_3-adrenergic agonist, CL214613. Starvation as well as leptin and dexamethazon influence the expression of UCP3. UCP3 mRNA is increased in muscle and decreased in BAT by starvation [32].

UCP3 was expressed in *E. coli* and reconstituted. Its transport characteristics were similar to characteristics of UCP2 and its role *in vivo* as mitochondrial uncoupler is predicted [29].

In a heterologous yeast expression system UCP3 was found to strongly impair the coupling efficiency of respiring cells thus resulting in increased thermogenesis. Uncoupling can also be demonstrated in isolated yeast mitochondria. Membrane potential of such mitochondria is decreased [32]. Contrary to what was observed with mitochondria containing UCP1, millimolar GDP and ATP had little if any effect on the uncoupling activity of UCP3 [36]. UCP3 increased the state 4 respiration by 1.2-fold in the isolated mitochondria. The growth of yeast expressing UCP3 was reduced. The growth rate was reduced by 49% and the whole O_2 consumption was increased by 31% [37].

2.3.4.3 PUMP

Plant uncoupling protein (stPUMP) from potato *Solanum tuberosum* is 306 aminoacids long, molecular weight is 32 000. PUMP is 44% homologous to human UCP1 and 47% homologous to UCP2. Protein is composed of three domains of 100 aminoacids each. Like in other uncoupling proteins each domain contains two transmembrane regions [38].

From *Arabidopsis thaliana* originates cDNA clone of AtPUMP. 306 aminoacids long protein is encoded by one gene in the genom. Homology to potato (*Solanum tuberosum*) PUMP is 81%. Expression of AtPUMP was proven to be cold inducible [39].

Another gene for PUMP in *Arabidopsis thaliana* was detected. This PUMP is marked as AtPUMP2. Despite the previous one, this gene does not respond to cold [40].

PUMPs from *Solanum tuberosum* as well as from *Arabidopsis thaliana* belong to group of plant uncoupling proteins from non-thermogenic plants. It is hypothesized that these PUMPs are predominantly associated with burst of respiration in flowering and fruit ripening [41,42].

In plant *Symplocarpus foetidus*[*] there were isolated two novel cDNAs encoding uncoupling protein: *Sf*UCPa c DNA encoding 303 aminoacids long putative protein with predicted molecular mass of 32.6 kDa and *Sf*UCPb cDNA encoding 268 aminoacid long protein with predicted molecular mass of 29.0 kDa. In the genome of *Symplocarpus foetidus* there is multi-copy dose of genes for *Sf*UCPa but just one copy of gene for *Sf*UCPb. *Sf*UCPa contains six predicted transmembrane domains and three MACP signatures plus PNBD close to the C-terminal end. *Sf*UCPb lacks the fifth transmembrane domain and third MACP signature [41].

PUMP, is similarly hydrophobic as UCP1. It is not retained on hydroxylapatite in a detergent micellar solution. Fatty acids regulation of PUMP exhibits the same characteristics as that of UCP1.

Purine nucleotide inhibition of PUMP is only weak [43,44].

[*] This Asio-Pacific perennial plant belongs to family *Araceae.* Its English name is Skunk cabbage, Czech name is *samoduť zápašná*. In Middle Europe it is sparsely cultivated in botanical gardens or in gardens in vicinity of castles.

A major difference between plant and mammalian uncoupling protein is that PUMP transports small hydrophilic anions such as Cl^- very slowly, if at all [43].

2.3.4.4 UCP4 and BMCP/UCP5

Two proteins from UCP subfamily were detected in brain – UCP4 and BMCP1 (stands for Brain Mitochondrial Carrier Protein) [45], which was later matched with one of isoforms of mRNA transcripts of UCP5 gene. Hence the BMCP1 encompasses group of isoforms of uncoupling proteins proven in brain and testis: in human there were detected three isoforms – L = long version, S = short version and SI = short version with insertion. L form corresponds to 325 AA long protein which, except one AA exchange of V 180, represents human BMCP1. This protein is 39% homologous to UCP3. In mice long form (L) and short form (S) were identified. Mice UCP5S is identical to mice BMCP1. BMCP1/UCP5 fulfills criteria of MACP proteins – the tripartite UCP architecture with six transmembrane α- helices; three mitochondrial transporter signature motifs are present. Also nucleotide binding site is present. Within BMCP1/UCP5 molecule exists unique hydrophobic 22 AA amino-terminal sequence that is not present in the other UCPs. Function of this sequence is speculated as possible membrane anchor. This 22 AA long sequence also contains a hydrophobic segment that may be involved in interaction with mitochondrial membrane. Northern blot analyses detected UCP5 in one of its isoform in a broad variety of organs, including kidney, uterus, heart, lung, stomach, liver, skeletal muscle, WAT, BAT. In agreement with previous knowledge, absolutely highest levels of expression were detected in tissues of brain and testis, among these organs. Predominant form in human brain is UCP5L whereas the mouse brain dominates short UCP5S [46].
BMCP1/UCP5 is 34% homologous to UCP1, 38% homologous to UCP2 and 39% homologous to UCP3 [45].

Uncoupling activity of UCP5 was proven in experiment in which human embryonic cells were transfected with expression vector carrying gene for UCP5. Potential was detected by fluorescent dye TMRE. Results confirmed previous findings that BMCP1 exerts uncoupling activity.

In experiments done in yeast with expressed BMCP1/UCP5, the growth was strongly slowed down. Moreover in yeast or yeast spheroplasts with expressed BMCP1/UCP5 the relationship between respiratory rate and membrane potential reveals marked uncoupling of respiration. This

can be understand as supportive “physiological” argument for “membership” of this protein in the UCP family, despite its relative sequencial distance from the cluster UCP1, UCP2, PUMP [45].

UCP4, protein 323 aminoacids long, is 34% homologous to UCP3, 33% homologous to UCP2 and 29% homologous to UCP1. Molecular weight of UCP4 is 36.061 kDa. Six putative transmembrane domains can be defined, as well as three mitochondrial transporter protein signatures and one PNBD. UCP4 maps to human chromosome 6p11.2-q12. Expression of UCP4 mRNA is in adults as well as in fetuses strictly limited to brain tissues. UCP4 is localized to mitochondria. Its etopic expression reduces mitochondrial membrane potential [47].

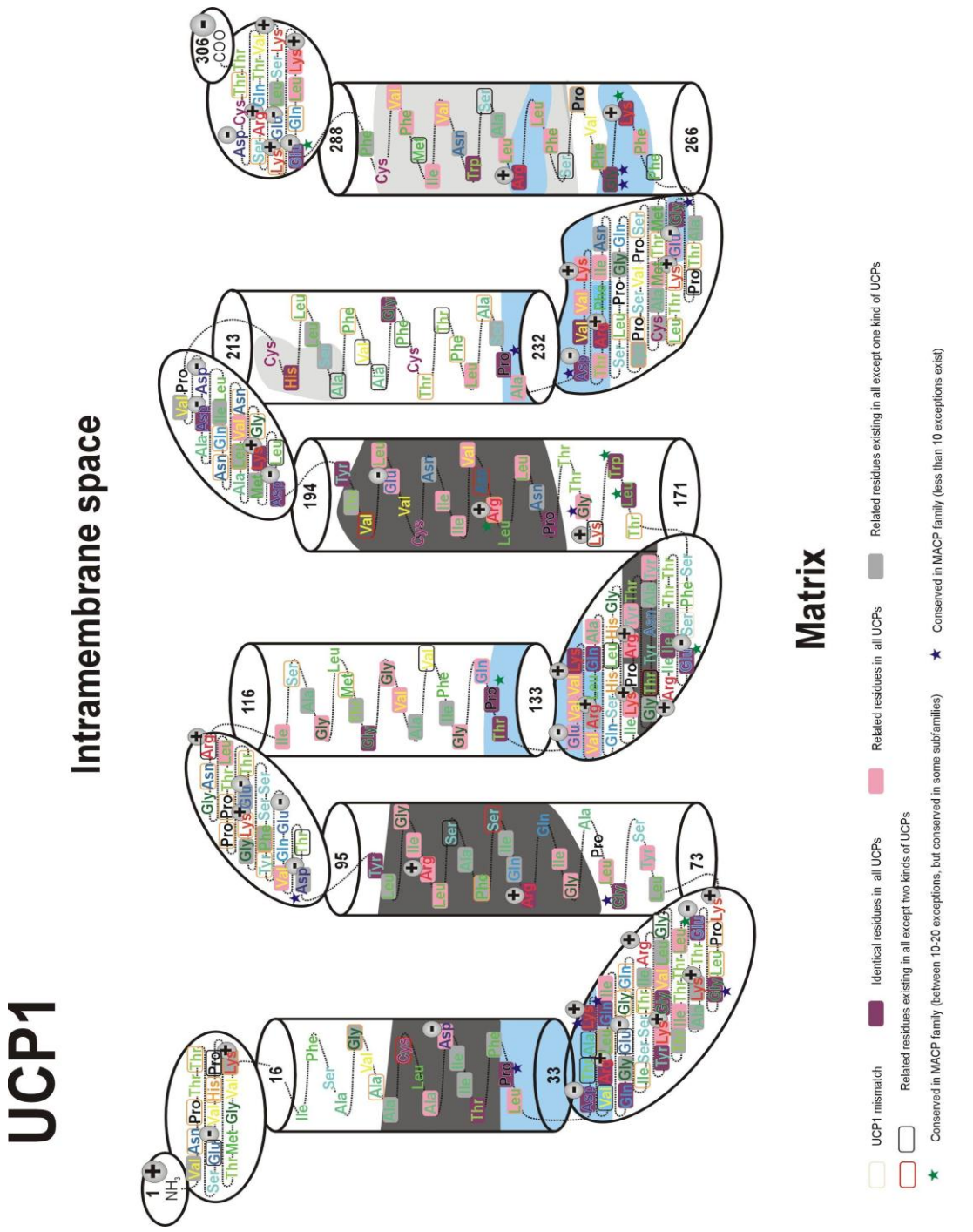

Fig.2: The transmembrane folding model of hamster UCP1 (SwissProt P 04575) according to Klingenberg. This model is based on tripartite structure of three roughly 100 amino acid long repeats and on common model of folding proposed for AAC and for UCP by (Klingenberg 1990).

2.4 UCP 1

Rat UCP1 is 306 aminoacid long, with molecular weight 33.042 kDa and polarity index (PI) of 42%.
UCP1 from golden hamster is 306 aminoacids long. Its molecular weight is 33.215 kDa, but the protein displays molecular weight 32.000 kDa according to polyacrylamide gel electrophoresis, PI is 43.5 % [17,48-50].
Human UCP1 is 305 aminoacids long, molecular weight is 32.786 kDa with PI 41%. Its structure probably consists of 50% α-helix, 28-30% β-structure, 13-15% β-turns and 7% unordered [51].
Structure of UCP1 is composed of three internally homologous domains encompassing roughly 100 aminoacids each. C and N ends face intermembrane space (cytosolic side). Each of three domains is composed of two membrane spanning α- helices separated by relatively hydrophobic stretch of 35 to 40 residues. This part faces the matrix side of the inner mitochondrial membrane while the connecting segments between α- helices on the cytosolic side are shorter [17].
UCP1 is considered to be a functional dimer [52].

UCP1 is encoded by gene *ucp*. Only one gene *ucp* is present in the (haploid) genome (the same situation is in the case of oxoglutarate-malate carrier).
In mouse the *ucp* gene is localized on chromozome 8.[53] Rat *ucp* gene is localized on chromosome 19 [54]. In human the most probable, if not sure, localization is on chromosome 4 [9,48,55].
Structure of *ucp* gene is characterized by „tripartite“ structure analogous to the structure of UCP1 – six exons are separated by five introns in a way that two exons separated by one intron compose one unit corresponding to one 100 aminoacid repeat of protein.
Transcription unit of rat ucp gene spans 8.4 Kb [9,55,56].

Human UCP gene spans 13 Kb and contains a transcribed region that covers 9 Kb of the human genome [55].

In rodents UCP1 mRNA exists in two lengths due to the existence of two polyadenylation sites. Occurrence of these two kinds of mRNA seems to have no functional importance [9].

The first identification of a putative UCP1 molecule was done by a photoaffinity labeling experiment in which an 8-Azido-adenosine [γ-^{32}P]triphosphate was prepared and covalently

bound to hamster brown-adipose-tissue mitochondria by near- ultraviolet irradiation. Two major radioactive bands were identified of apparent molecular weight 30 kDa and 32 kDa. Selective labeling identified 32 kDa protein as the regulatory site of the energy- dissipating ion uniport [57].

Independently, a 32 kDa protein, abundant in the membranes of BAT mitochondria was described. This protein was induced during exposure of rats to the cold and down-regulated after re-adaptation to room temperature [50].

The isolation of a UCP1 molecule was first successfully performed by two poly(oxoethylene)-type detergents: Emulphogen BC 720 and Triton X-100. The latter has become the routinely used tool. In spite of isolation of ADP/ATP carrier, nearly no salt is necessary for the Triton isolation. GDP binding of the isolated UCP1 can be used as the criterion of its biochemical and biological activity. Biochemical activity is retained for at least 7 days at 0 ^{o}C but only 1 – 2 days at room temperature. In liquid nitrogene the native status lasts more than 14 months [49].

One of models of UCP molecules highlights the domain character and function of sections spanning the transmembrane α- helices on their matrix ends. There are three such domains, connecting the first α-helix with the second, another domain connecting the third α-helix with the fourth and the last one connecting fifth and sixth transmembrane helices. To establish the secondary structure of the last matrix –facing domain between the fifth and the sixth transmembrane helices, the peptide corresponding to residues 261 to 269 was synthesized. Circular dichroism studies which have been done on it show presence of α-helical structures in the extent of 26 %. Nuclear magnetic resonance confirmed presence of α-helices in particular population of these peptides [58].

Newly synthesized UCP1 has (with one exception of methionine at the N-end) no leading sequence. Information for targeting and integration into mitochondria is encompassed mainly in first one hundred AAs. Targeting mechanism is quite versatile as UCPs translated *in vitro* or originating in phylogenetically distant organisms are integrated in proper way. It seems probable that UCP1 molecules, unlike other proteins do not traffic via matrix compartment when being incorporated. One week halftime of UCP1 is the same as the duration of halftime of the inner mitochondrial membrane [9].

2.4.1 Function of UCP1

UCP1 exerts fatty acid-activated and purine nucleotide inhibited uncoupling of mitochondria.
Not only H^+ is translocated by UCP1. Also monovalent unipolar anions are transported by UCP1 [59], namely halides [60].
Another transported category is nonphysiological anions such as alkylsulfonates and monovalent phosphate analogs [59] as well as physiological ketocarboxylates, such as pyruvate [61].

UCP1 is also characterized by binding of purine nucleotides. Binding is highly specific for di- and triphosphates. Affinities are slightly higher for guanosine derivatives than for inosine derivatives. Affinities of monophosphates are lower by two orders of magnitude. Nucleotide binding is diminishing by increasing concentrations of salts [49].

The GDP-binding capacity is lost in mitochondria from UCP1-ablated mice. Addition of GDP was without effect on energization of such mitochondria [62].

Inhibitory action of purine nucleotides is accompanied by conformational change of UCP1 molecule: Antagonist DAN-ATP (which binds to the nucleotide binding site) exhibits much more rapid binding than ATP. This is explained by undergoing conformational change accompanying ATP binding [9,63]. Decrease in fluorescence as well as changes in infrared spectra upon GDP binding also indicate conformational change of UCP1 [9,51,64].
Also trypsin or chymotrypsin digestion of UCP1 slows down binding of GDP by altering PNBD [65]. On the other hand binding of nucleotides changes pattern of degradation products. This also indicates conformational change caused by GDP [9,65,66].

On theoretical base four models of transport function of UCP1 were postulated:
In first model two permeabilities are suggested – one for protons, another one for Cl^-. Both of them are inhibited through one purine nucleotide binding site [60,67]. Fig. 3a).

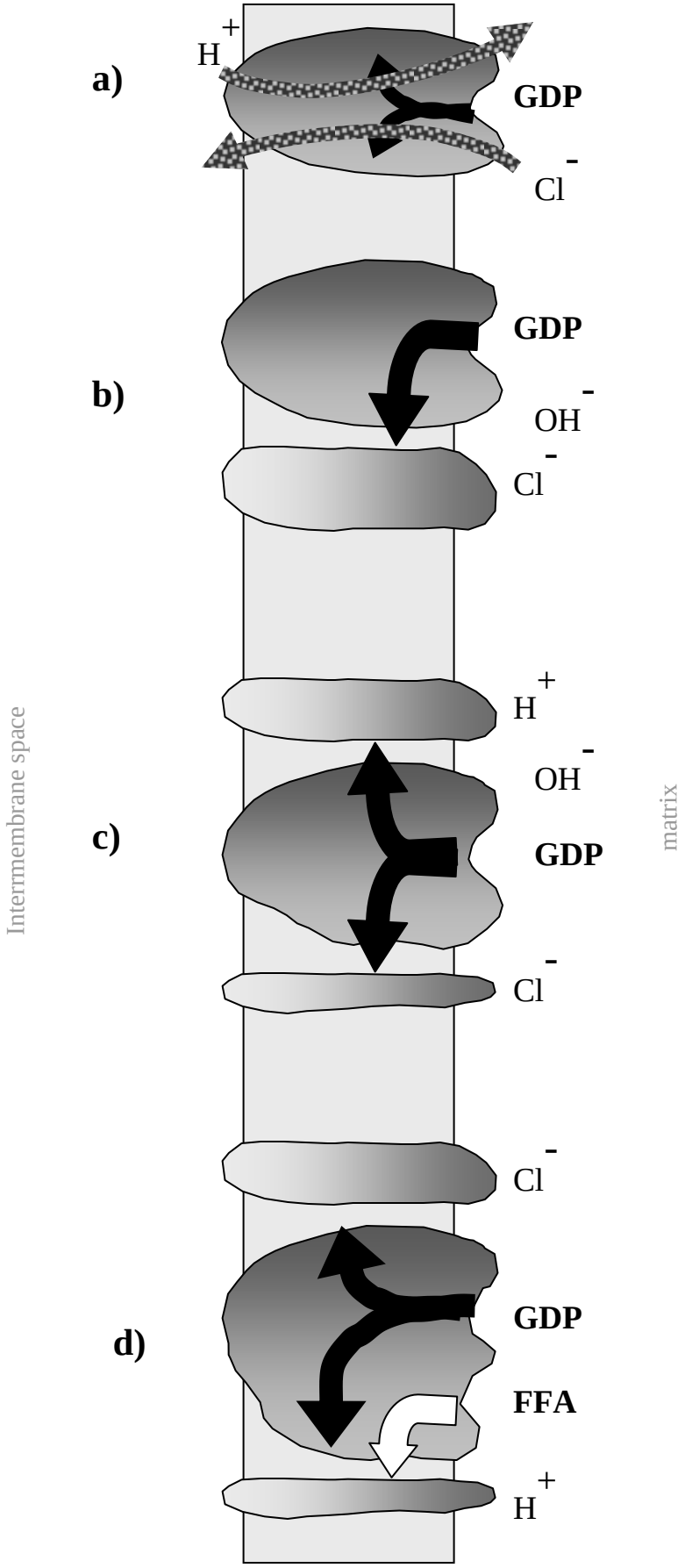

Fig.3: Four proposed mechanisms of UCP1 transport function. a) one permeability for both H^+ and anions. b) shunting by means of OH^-; one permeability common for all anions. c) separated permeabilities for H^+ and anions, but with one common inhibitory binding site for PNs. d) separated permeabilities for H^+ and anions. Just permeability for H^+ is stimulated by FAs. Inhibitory binding domain for PNs is common to both permeabilities.

In another model the uncoupling function is performed by OH^- ions, hence only one permeability, common to boths Cl^-. and OH^- is needed. This permeability is regulated by one purine nucleotide binding site [68]. Fig. 3 b).

This was supported by observation that Cl^- as well as OH^- competed for this path and also that there was identical sensitivity of both of these transports to purine nucleotide inhibition [60,69-71].

On the other hand later observations showed difference in sensitivity of OH^- and Cl^- transport to inhibition by purine nucleotides [72,73]. Third model was suggested to cope with these later observations: There are two different permeabilities – one for Cl^- and another for OH^- and H^+. Fig. 3c). Both of these permeabilities are inhibited by purine nucleotides bound to one common binding site. Problem with this model is that it is not simple to discriminate between H^+ and OH^- data.. Inhibition of Cl^- by purine nucleotides is easier than inhibition of H^+ transport [72,74]. On contrary to this, another group found H^+ permeability inhibitable in easiest way than Cl^- permeability. These results were obtained from experiments in which swelling was used as measure of transport of both of these substrates [75].

Fourth model copes with the observation that fatty acids positively stimulate H^+ transport but not transport of Cl^- [76]. Two separate permeabilities are suggested – one for halides and the other one for H^+ . One binding place for inhibitory purine nucleotides common to both permeabilities is suggested plus another separate binding site for fatty acids. This FA binding site influences just permeability for H^+ . Fig. 3d).

Two theories how fatty acids facilitate H^+ transport were postulated: according to one model UCP1 actually transports protons and fatty acids provide an essential free carboxyl group making proton transport possible or more efficient. Existence of H^+ translocation pathway within the structure of UCP1 is considered. FA-activation of UCP-mediated H^+ transport is explained by a concept of local buffering predicting that ionized FAs somehow participate in or facilitate jumps of H^+ over an array of sites (certain amino acid residues) that form their translocation pathway [77].

Model of fatty acid cycling suggests that charged fatty acids interact in the same binding domain as other anions do. Translocation of fatty acid anions then leads to FA cycling [42,78,79]. Anionic fatty acid is protonated on the other side of the membrane (the cytosolic side *in vivo*) and, in the form of a neutral FA, returns by flipping back across the lipid bilayer. Fig. 4.

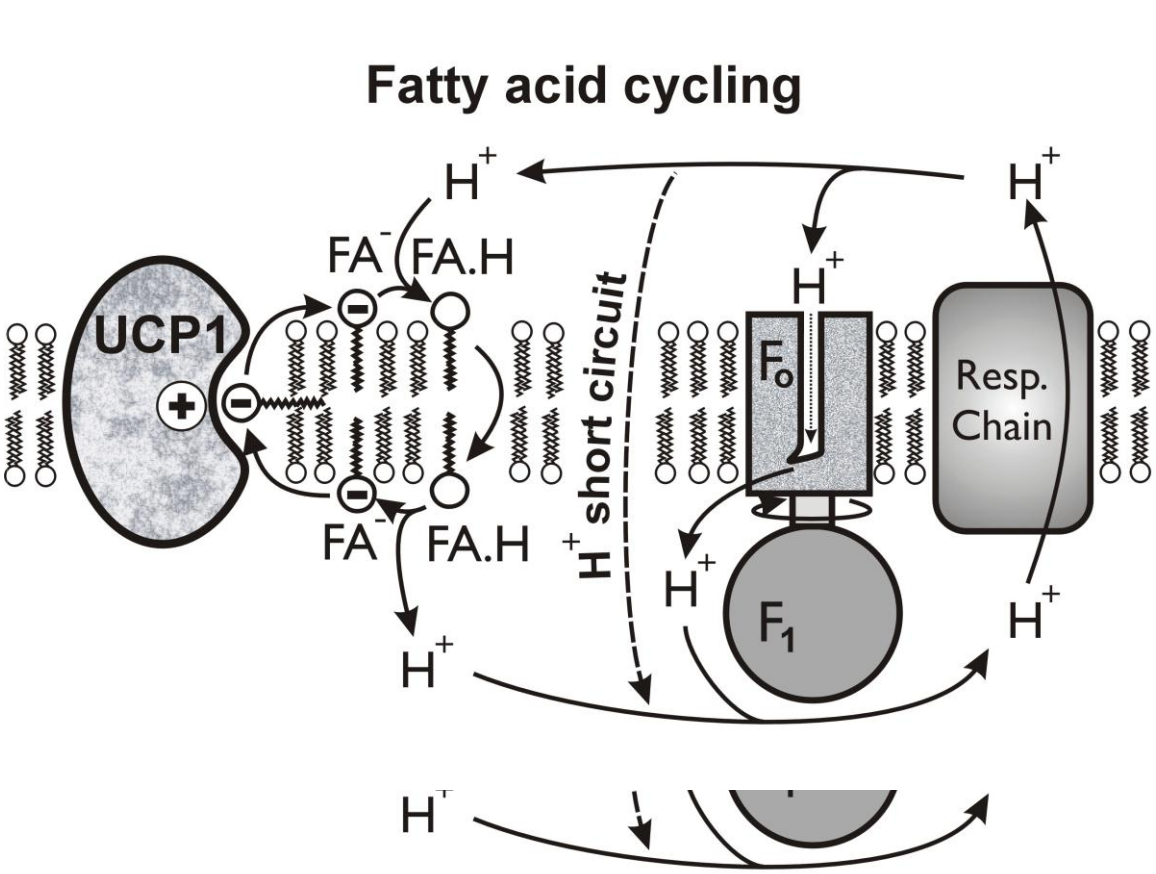

Fig. 4: Fatty acid cycling provided by UCP1. Neutral (protonated) FA flip-flop from intermembrane side of the inner mitochondrial membrane (in order to retain equilibrium of neutral FAs between the two lipid sheets of the membrane) to the other side of the membrane. Some of them then deprotonate on the matrix side and thus protons are transported. FA anions are transported by UCP through the membrane. In order to retain equilibrium between FA^- and neutral species, some of them accept protons and become neutral, thus capable freely pass through the membrane.

Its dissociation releases H^+ and the resulting FA anion can enter the cycling again until all non-esterified FAs are combusted or depleted. The major support for FA cycling has been brought in the past by the demonstration that so called inactive FAs that are unable to flip- flop across the lipid bilayer, are also unable to induce H^+ transport with UCPs [80,81]. Thus, inhibiting flip-flop, one observes an inhibition of UCP- mediated H^+ uniport.

2.4.2 Mutations influencing UCP1 function

2.4.2.1 Mutations influencing nucleotide binding

Nucleotides regulating the function of UCP are polyanions, so that positively charged aminoacids are supposed to be counterparts in the predicted nucleotide binding site. Numerous mutational exchanges of various residues in UCP1 have been done. The extent of impairment of nucleotide binding functions was tested on following exchanges:

Arg 276 from the 6^{th} transmembrane α-helix was substituted by Leu. This substitution abolished sensitivity of H^+ transport to GDP inhibition [82].

Positively charged residues Lys 72, Lys 268, His 214, Arg 83, Arg 182 and Arg 276 were mutated and the influence on transport as well as on the nucleotide binding and inhibition were measured. Mutants Lys 72 Gln and Lys 268 Gln did not perform neither any significant change in nucleotide binding, nor inhibition of proton flux in reconstituted proteoliposomes when compared to wild type UCP1.
In Arg 83 Gln mutant, Arg 182 Thr mutant and Arg 276 Leu mutant, the nucleotide inhibition of proton transport was abolished. In agreement with this binding of purine nucleotides to Arg 83 Gln and Arg 182 Thr was abolished too [83].
Surprisingly the binding of Arg 276 Leu mutant was untouched [82].

From these results the following conclusions can be considered:

Different binding sites are used for fatty acid induced transport and for inhibitory binding of purine nucleotides.

Transmembrane helices II., IV. and VI. are involved in nucleotide binding. They can form „walls" of dead end nucleotide binding site.

Sugar-base moiety of nucleotide binds to the matrix loop spanning fifth and sixth transmembrane helices. This could be critical step for discrimination between purine and pyrimidine nucleotides. (The second category does not inhibit transport functions of UCP1). Nucleotide β-phosphate binds to Arg 182 [84].

Tight conformation of UCP1 is characterized by interactions of nucleotide with Arg 83 and His 214.

In inhibited stage Arg 276 binds to α- phosphate of nucleotide [84].

In another experiment His 214 was substituted by Asn and by Trp. Data from experiments done with these two mutants show striking difference in dynamics of NTP (but not of NDP) binding affinity according to pH between wild type UCP and each of the mutants. The K_D values change in pH range 6.8 – 7.5 8 fold in wt, 1.5 fold in His 214 Asn and almost do not change in His 214 Trp UCP1. Independently on this, the pH dynamics of K_D value for NDP is not influenced in any of both His 214 mutants.

Kinetic study of GTP binding in wt and both of His 214 discussed mutants confirmed the results obtained with NTP binding. K_D: k_{on} differs in pH range 6.5 – 7.5 7-fold in wt, but only 1.4-fold in mutants. k_{off} rate determined by dansyl-GTP titration is in accordance with the k_{on} data.

Results of these experiments show importance of His 214 in NTP binding to UCP1. As interconnected with pH dependence of such binding **His 214 seems to serve as the part of a sophisticated regulatory mechanism of uncoupling** and thermogenesis. [85].

Also His 214 to Gln mutant was constructed. Functional characteristics of this protein seem to contradict the role of this residue in the regulation by NTPs.

Impairment of carboxyl group of **Glu 190** in hamster UCP1 leads to the UCP molecule with decreased or abolished pH control of regulatory nucleotides binding: This substitution leads to increase of GTP binding at higher pH, confirming its **role as pH sensor** of nucleotide regulatory mechanism [86].

Two aspartic acid residues Asp 209 and Asp 210 provide negative background for His 214. According to the extent of the negative charge of Asp 209 and Asp 210, which is in relation with pH, the His 214 is positioned or in the way preventing insertion of γ-phosphate of NTP into binding site or in the position allowing it. Mutagenic elimination of COO^- groups in Asp 209 and Asp 210 (Asp 209 Asn, Asp 210 Asn and double mutant Asp 209 Asn + Asp 210 Asn) led to decreased affinity for NTP binding. This effect was more expressed in Asp 210 and double mutant. The binding of NDP and dependence of this binding on pH remained unaffected [87].

The current model of NP binding site is based on following building blocks:

1) COO^- group of Glu 190. This group controls the entrance into the binding site by forming (or not) anion pair
2) His 214 which protrudes from the „bottom" into the binding niche and sterically prevents entrance of γ-phosphate of TNP.

3) Asp 209 and Asp 210 residues providing at particular pH negative background to His 214 and drawing it out from the binding niche [87].

Sequence 261-269 of the UCP1 is highly homologous to sequences in the DNA binding domain of the estrogen receptor and in the adenine nucleotide translocator. This putative nucleotide recognition element spanning amino acids 261-269 of the UCP1 was gradually impaired, and resulting mutant proteins were expressed in yeast. Increased uncoupling activities of such mutant proteins were detected by measuring the mitochondrial membrane potential by flow cytometry. The deletion of three amino acids Phe267, Lys268 and Gly269 resulted in a mutant in which proton leak could be activated by fatty acids but not inhibited by nucleotides [88]. Deletion of amino acids 261-269 converts the UCP1 molecule into an unspecific pore [89].

2.4.2.2 Mutations influencing H^+ transport and Cl^- transport

First attempts to analyze UCP1 transport functions by site-directed mutagenesis were done on cystein residues to test models of transport involving essential thiol groups. Cysteins in positions Cys 24, Cys 188, Cys 213, Cys 244, Cys 253, Cys 287 and Cys 304 were substituted by Ser. Except elimination of the thiol group serine keeps the polarity and bulkiness of the residue.

Examination of swelling, respiration and GDP binding did not show any significant change when compared to wild type. Hence, importance of residues with thiol groups for transport was dismissed [90].

When His 145 and His 147, residues in second matrix segment, were neutralized by mutation into residues Gln and Asn the H^+ transport function was diminished to roughly 20 % of value common in wt proteoliposomes. In this mutant the rate of inhibition by nucleotides is proportional to the nucleotide inhibition in the wild type UCP1 showing that His 145 and His 147 are not involved in nucleotide binding. In proteoliposomes reconstituted with double mutant carrying His 145 Gln together with His 147 Asn mutation the transport is in fact abolished.

Cl^- transport has not been influenced by any of His 145, His 147 or double mutation. Autors of communications dealing with these mutagenic impairments of **His 145** and **His 147** residues use this **discrepancy** in influence of these mutations to **H^+ compared to Cl^- transport** as the **argument against the fatty acid cycling** theory [91].

Interesting results were obtained from substitution of Glu at position 167. Neutralization of negative charge of Glu by substitution with Gln does not affect the H^+ transport function, while Cl^- transport activity was almost abolished [87]. Conclusion that this residue playes important role in anion translocation is a bit relativized by its presence in plant UCPs which do not transport Cl^-.

Asp 27 residue, the only residue in first signature possessing negative charge, seems to play important role in UCP facilitated H^+ transport due to its COO^- group. There is striking difference in H^+ transport between mutation of Asp 27 Glu still carrying the carboxyl group and Asp 27 Asn, where there is amidic group present on the place of carboxyl group of the wild type UCP1 molecule. While in the Asp 27 Glu mutant the H^+ transport is decreased slightly in reconstituted system, the Asp 27 Asn mutation causes almost complete inhibition.

Asp 210, residue in the third cytosolic segment, which is believed to be one of players in the regulation of uncoupling by nucleotide binding also takes part in the H^+ transport function as the abolishment of its COO^- group by mutating into Asn 210 affects the transport as well as the regulatory function [87]. Interpretation is relativized by the fact that this aminoacid (negative charge, generally speaking) does not occur at this position neither in UCP3 nor in UCPs of lower multicellular organisms.

His 214 Asn and His 214 Trp mutations, which play role in regulatory binding of TNPs, were also examined to exclude their possible involvement in transport function. Summary of these results really excluded functioning of His 214 in transport.

The transport properties of UCP1 have also been studied in mutants where Cys304 has been replaced by either Gly, Ala, Ser, Thr, Ile or Trp. Cys 304 is localized in the region of C-terminus of UCP1. This place faces cytosolic side of the mitochondrial inner membrane.

Substitution of Cys304 by non-charged residues alters the response of UCP to fatty acids. The most effective substitution is Cys for Gly since it greatly enhances the sensitivity to palmitate. On the contrary substitution by Ala increases twofold the half- maximal concentration. These results show that C-terminal region participates in the fatty acid regulation of UCP activity [92].

mutation	type of substitution	H^+ transport	Cl^- transport
Cys 24 Ser, Cys 188 Ser, Cys 213 Ser, Cys 244 Ser, Cys 253 Ser, Cys 287 Ser, Cys 304 Ser (Arechaga, I. *et al.,* 1993)	elimination of thiol group	no effect	
His145Gln (Bienengraeber, M. *et al.*, 1998)	neutralization of positive charge	20% of wt	no effect
His147Asn (Bienengraeber, M. *et al.*, 1998)	neutralization of positive charge	20% of wt	no effect
His145GlnHis147Asn (Bienengraeber, M. *et al.*, 1998)	neutralization of positive charge	almost abolished	no effect
Glu167Gln (Echtay, K. S. *et al.,* 2000)	neutralization of negative charge	no effect	almost abolished
Asp27Glu (Echtay, K. S. *et al.*, 2000)	exchange within COO^- AAs	slight decrease	
Asp27Asn (Echtay, K. S. *et al.*, 2000)	substitution of COO^- group by $CONH_2$	almost abolished	
Asp210Asn (Echtay, K. S. *et al* ., 2000)	substitution of COO^- group by $CONH_2$	20% of wt	
Asp209Asn (Echtay, K. S. *et al.* , 2000)	substitution of COO^- group by $CONH_2$	80% of wt	
His 214 Asn, His 214Trp (Echtay, K. S. *et al.* , 1998)	neutralization of positive charge	no effect	

Tab.1: Overview of prepared AAr substitutional UCP1 mutants and the influence of the substitution onto the transport characteristics of the molecule.

2.4.3 Molecular regulations

Protonophoric function of UCP1 is activated by fatty acids and both protonophoric function and transport of monovalent unipolar anions are inhibited by purine nucleotides. Nucleotide binding and inhibition strongly decrease with increasing pH. Below pH 6.4 PN nucleotide binding is constant [49]. In the pH dependence break occurs at pH 6.4, above which approximately 10 fold increase in K_d originates with increase pH by 1 unit. Nucleotide triphosphates have another break in the pH dependence above which this dependence is 2 times steeper.

First indications of molecular interaction of UCP1 with fatty acids was the observation that the extent of thermogenesis induced in mitochondria after addition of fatty acids is proportional to the amount of UCP1 in cells.

Addition of GDP inhibits the fatty acid activated H^+ transport but not the uncoupling effect of artificial uncoupler FCCP, the action of which is independent of UCP1. Thus, fatty acids interact specifically with UCP1 but at a different site than purine nucleotides [9,76]. Free fatty acids probably do not influence conformation of UCP1 as shown by infrared spectra [51].

With increasing pH (decreasing H^+ concentration) the nucleotide inhibition decreases (increasing values of K_I for H^+ transport inhibition and of K_D for nucleotide binding). This pH dependence is more expressed in GTP and ATP (triphosphatidic nucleosides) than in diphosphatidic nucleosides. CO_2H group of **Glu 190 is believed to be the first pH sensor of NDP as well as of NTP binding, while His 214 functions as an exclusive pH sensor of NTP binding** [85-87,93,94]. It seems to be clear that only this two-step mechanism can guarantee fine pH sensitivity (in quite narrow pH range) for the key inhibitor – ATP.

At least two steps in nucleotide inhibition of UCP are proposed. In the first stage, the nucleotide binds by a loose bond in the transitional way. At this stage the transport functions of UCP are not influenced. Then it slowly proceeds into tight binding which encompasses conformational changes of the protein.

There is a general agreement that the binding site for regulatory nucleotides is distinct from transport channel.

Gonzalez-Barroso et al. suggest interesting model dealing with two modes of uncoupling regulation. At **low concentration of fatty acids**, generated by hormone-sensitive lipolysis the H^+

transport is induced. This is **the situation of UCP1 driven uncoupling in vivo**. At much **higher concentrations of fatty acids transport of anions** is stimulated [95].

Problems with reconstitution of UCP1 produced in inclusion bodies of *Escherichia coli* led to the speculation that some cofactor is necessary for its full function. Series of experiments in which chromatographic fractions of extracts from mitochondria with translated UCP1 as well as without it (bovine hart mitochondria) revealed, in combination with UV spectrometry, that the coenzyme Q is the activating agent. Regained transport was inhibited by purine nucleotides, and it was concluded that is facilitated by UCP1. Further experimental results show that only oxidated form of CoQ interacts with UCP1. Hence, the redox state of CoQ can play a role as a regulatory factor of uncoupling [115] .

Data obtained on murine gene show three basic areas of regulation of UCP1 expression in response to norepinephrine or cold:

1) Promotor region extending from start of transcription to –272 bp, encompassing TATA box and cAMP response element – here marked CRE4. CRE4 has been proven to be active in expression regulation – playing role in promotor function.
2) Silencer located in interval –272 to –900 bp.
3) Enhancer situated at about 2600 bp upstream from the transcription start. This enhancer carries three cAMP response elements – CRE1, CRE3 and CRE2, characterized by CGTCAC motif. Data obtained from mutagenic modifications of particular CREs, followed by evaluation of the level of expression of reporter gene show, that CRE1 is quite unimportant in UCP1 expression, CRE3 has 15 – 50% influence and CRE2 is of critical importance. CRE2 is followed in downstream direction (still within the functional unit of enhancer) by two "brown fat regulatory elements" BRE1 and BRE2, characterized by motif TTCC. **BRE2** seems to be **responsible for tissue specific expression of UCP1 gene in BAT**. Binding of heterodimeric complex of nuclear proteins, in which one moiety is CREB (stands for CRE Binding Protein) to the CRE2 – BRE1 motif was speculated [96]. Upstream of CRE2 – BRE1 motif at position –2478 to –2490 is situated response element of peroxisome proliferation activating receptor γ_2 (PPARγ) – PPARE referred to as UCP regulatory element 1 (URE1). This sequence binds PPARγ - RXR heterodimers. It acts in transduction of one stimuli in quite complex regulatory mechanism [97,98].

Enhancer sequence of rat UCP was also extensively studied. Length of this sequence is 211 bp, situated 2280 bp upstream of the transcription start. Thyroide hormone response sequence

(THRS) is located between 2317 and 2399 bp upstream. Characteristic for this sequence is motif AGGGCAgcaAGGTCA. The sequence binds $\beta_1 T_3 R$ or combination of $T_3 R$ with retinoid X receptor (RXR). Another TRE is situated 27 bp from the first one [98,99].

The mechanism of (co)stimulation of UCP1 expression by T_3 is based on substitution of homodimer of $T_3 R$, unoccupied by ligand, which acts in repressive way, by heterodimeric $T_3 R$ – RXR. T_3 stimulates this exchange. There is difference in affinity to homodimeric $T_3 R$ ligand and heterodimeric $T_3 R$ – RXR between each of both TREs. The TRE proximal to transcription start prefers heterodimers, hence acting in more stimulatory manner. The distant TRE displays quite opposite tendency and in fact serves as "threshold sensor"

Structure homologous to the mouse sequence encompassing CRE2 – BRE1 sequence is in the rat gene located in position –2399 to –2490, named R90 [98]. Three pairs of retinoic acid response elements (RARE) are located within the sequence R90, marked up-90, mid-90 and dn-90. It was proven that up-90 and mid-90 bind RAR receptor in homodimeric (RAR)γ as well as heterodimeric (RXR) forms. Mid-90 forms antiparallel strand to part of CRE2 – BRE1 rat homologous sequence.

Two binding sites for CCAAT/enhancer binding protein (C/EBP) α and C/EBP β were located at positions –457 to -440 and –335 to-318 [8].

2.5 Heterologous expression of UCP

Several attempts to produce UCP1 in an experimental way in various organisms were done. One approach was based on expression system in mammalian cell lines. In ovary cells of Chinese hamster was expressed UCP1 detected in mitochondrial fraction, thus proving insertion of the protein into mitochondria. The content of protein was however too low to allow isolation and functional characterization of the protein [100].

Attempts to express UCP1 in oocytes of African clawed frog (*Xenopus laevis*) were unsuccessful [101].

UCP1 was expressed in bacteria *Escherichia coli* under the control of galactose or temperature-sensitive promotor. In both of these biotechnologies quite high yield of UCP1 was obtained, but without success in reconstitution of protontransport activity after incorporation into liposomes. [77]

Yeast strains are frequently used for expression of proteins from another organisms [102-107].

Expression system based on 2 μ circular shuttle vector *E. coli* / *S. cerevisiae* with integrated rat *Ucp1* gene was constructed in Freeman´s laboratory [71]

3 Methods

3.1 Genome and protein database search

Protein or DNA sequences of new members or candidate members of UCP family were searched according to their homology using Blast function. Accessible databases such as Fly Base (www.fruitfly.org/blast/), DictyDB (dicty.sdcs.edu/), *C. elegans* Blast Server (www.sanger.ac.uk/Project/C_elegans/blast_server.shtm) or SRS6 hub (srs6.ebi.ac.uk) were used. The core reference UCP sequences were those of hamster UCP1 (P04575 in SwissProt) and human UCP1 (SwissProt P 25874), human UCP2 (Gene Bank accession number U76367, SwissProt P55851), human UCP3 (SwissProt P55916), human UCP4 (NM004277.1 or SwissProt O95847), BMCP1 (AL035423.4 or SwissProt O95258) and PUMPs: StUCP (Y11220) and *At*PUMP1 (EMBL AJ223983) and *At*PUMP2 (EMBL AB021706).

Computer alignment was performed using Clustal method (MegAlign program of the Lasergene 99 sequence analysis system), applying the Dayhoff PAM 250 matrix. Function "percent similarity" of the MegAlign program was employed to assess similarities between various segments of sequences. When the final phylogenetic tree was constructed from already annotated sequences the Jotud Hein method was employed.

3.2 Construction of mutated UCPs

The whole process of construction of UCPs with substituted AA residues consisted of sequence of procedures listed in Fig. 5.

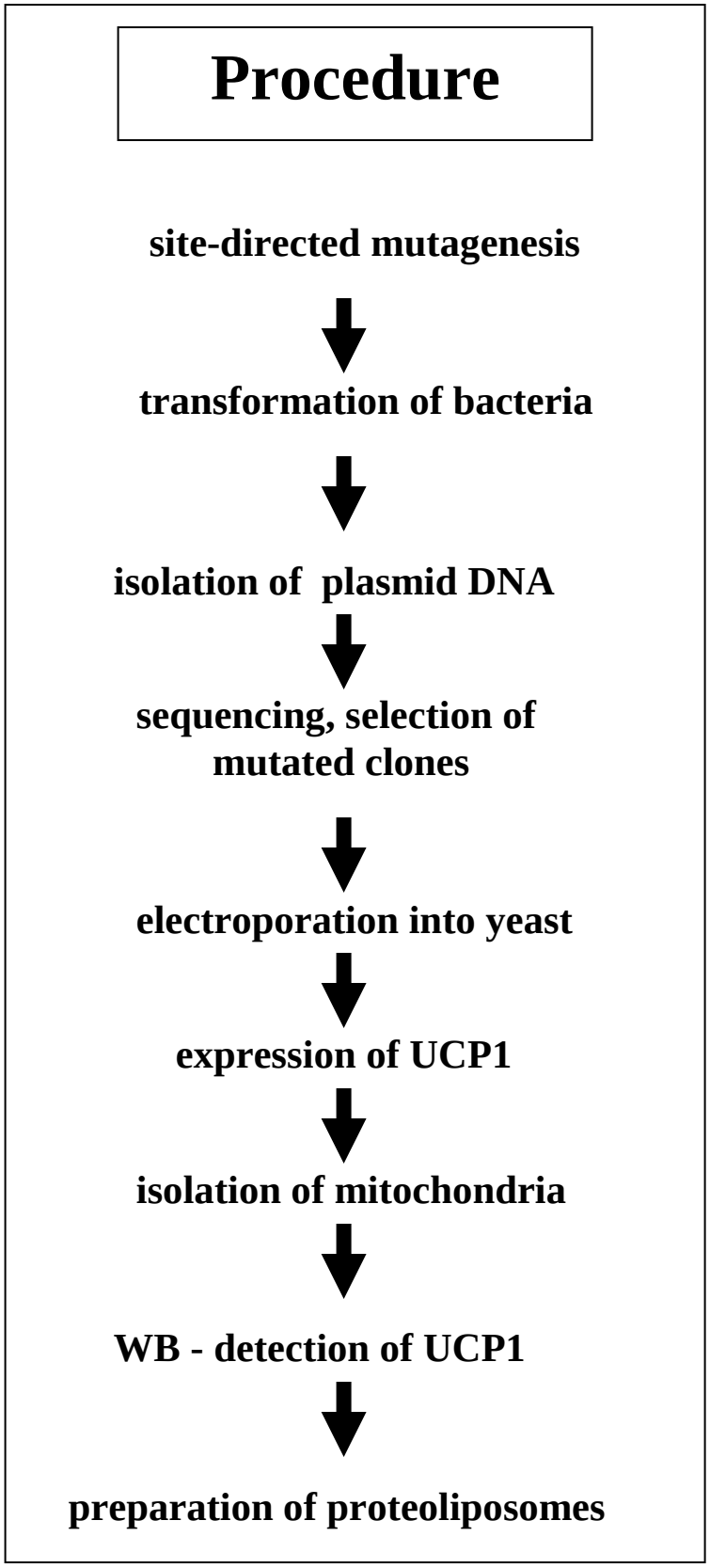

Fig.5: Scheme of sequence of experimental processes leading to artificial liposomes with molecules of mutated UCP1 species incorporated into the membrane.

3.3 Site-directed mutagenesis

3.3.1 Shuttle vector

Saccharomyces cerevisiae/*Escherichia coli* multicopy shuttle vector pCGS110 was used as the carrier of rat UCP1 cDNA. The 7.4 kb long plasmid was originally constructed from bacterial plasmid pBR322. This vector enables QuikChange version of PCR-based site-directed mutagenesis on dsDNA, propagation of *Dpn* I-digestion treated product in *Escherichia coli* and propagation and subsequent galactose- triggered expression of UCP1 gene in yeast *Saccharomyces cerevisiae* strain JB 516.

To fulfill these functions vector pCGS110 contains ampicilin resistance gene (Ap) which enables selection of successfully transformed bacteria on ampicilin (carbenicillin) solid media; bacterial origin of replication (ori); segment of the endogenous yeast 2 μ plasmid; yeast URA3 gene encoding orotidine-5´-phosphate decarboxylase making growth on uracil deficient (ura^-) media possible, and inducible GAL 1 promoter. To increase the level of expression of UCP1 in yeast, the 18-nucleotide upstream and 5-nucleotide downstream region around the initiating ATG of UCP1 cDNA was altered to resemble the sequence of a highly expressed yeast glyceraldehyde-3-phosphate dehydrogenase gene. Also certain codons were altered into yeast frequently used codon variants [71]. Fig. 6.

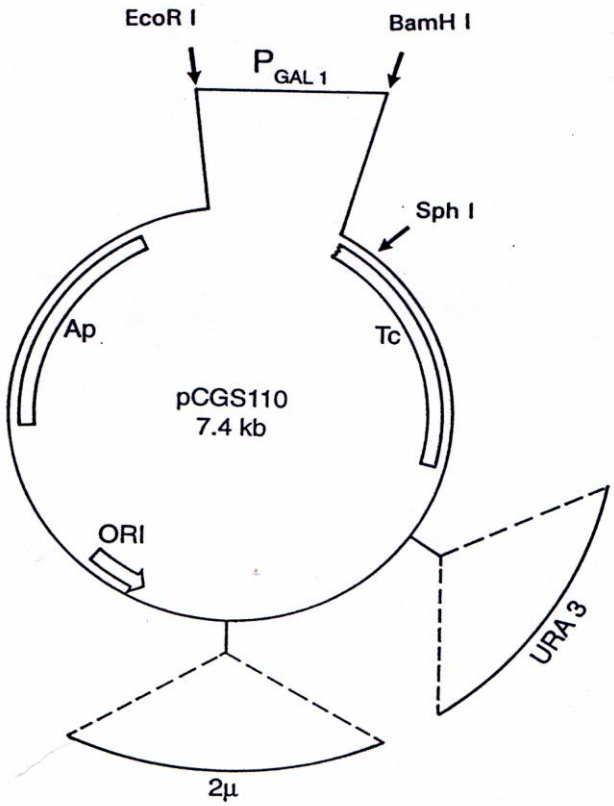

Fig. 6: *Saccharomyces cerevisiae*/*Escherichia coli* shuttle vector pCGS 110. This vector was constructed from the bacterial plasmid pBR322, with additions of the yeast inducible promoter GAL 1, a segment of the endogenous yeast 2 μ plasmid and the yeast URA 3 gene encoding orotidine –5′-phosphate decarboxylase. It also contains bacterial origin of replication (ori) and ampicilin resistance gene (Ap). Restriction sites EcoR I, BamH I and Sph I are marked by arrows.

3.3.2 Primer design

Mutagenic primers introduce specific experimental mutation. Proper design of mutagenic oligonucleotides is critical to the efficiency of the reaction. There exist general rules for the design of mutagenic oligonucleotides, but besides obeying these rules, each designed primer must be approached individually. Process of primer designing can be eased by using some of commonly available Internet sites which help with computation of parameters like T_m, CG content etc. For purposes of this work the site with URL: www.williamstone.com/primers/javascript/primers.cgi was used. UCP1 sequence was pasted into data entry box; region of interest and desired length were defined.

The mutagenic oligonucleotide must hybridize efficiently to the template. To ensure this, absolute base pairing at both ends of the target sequence, without secondary structure formation, is required.

One of the most important parameters for primer design is the total length of the oligonucleotide. In case of one mismatch present in the oligomer the value of the parameter should be at minimum 20 – 25 bp. Length of the primer is also in relation to the melting temperature (T_m). For particular setup of QuikChange method used in this work the minimal T_m was 78 °C.

In theory, the longer the primer, the higher T_m. On the contrary, the higher the number of mismatches, the lower T_m. Hence, with increasing number of mismatches the necessary length of the designed oligonucleotide goes up.

Primers were designed in a way that the desired mutation(s) were in the middle of the primer length at minimum 10 – 15 bp of correct sequence on both sides.

The GC content of designed primers was taken into account and used in computation of T_m. Also the tendency of oligomers to form secondary structure was checked and oligomers with such feature were avoided.

Primers were ordered in Generi Biotech, Czech Republic. Purity of primers was OPC (Oligonucleotide Purification Cartridge, which is comparable to HPLC quality).

Tab. 2. lists primer parameters.

mutation	number of missmatches	Tm - williamstone	Tm - QuikChange	Tm A	Tm B	%GC	primer length [bp]	sequence of mutagenic primers
His147Asn	1		71.03			56.50	23	5´ GGGTTTGATCCCGTTCAGATGGC 3´
								5´ 5´ GCCATCTGAACGGGATCAAACCC 3´
Arg152Leu	1	82.10	82.85	61.40	64.20	58.80	34	5´ GCACGGGATCAAACCCCTCTACACTGGGACCTAC 3´
Lys150Ile	1	84.71	84.05	62.60	65.40	61.80	34	5´ CCCAGTGTAGCGGGGTATGATCCCGTGCAGATGG 3´
								5´ CCATCTGCACGGGATCATACCCCGCTACACTGGG 3´
Tyr153Phe	1	80.27	82.77	61.20	64.00	57.10	35	5´ CATTGTAGGTCCCAGTGAAGCGGGGTTTGATCCCG 3´
								5´ CGGGATCAAACCCCGCTTCACTGGGACCTACAATG 3´
Thr30Ala	1	81.94	85.15	63.50	66.40	62.90	35	5´ GCTGGCATCCAGAGGGAAATCAGCTTTGCTTCCCTC 3´
								5´ CGGTGTCCAGCGGGAAGGCGATGATGTCTGCTAGG 3´
Asp27Val	1	81.57	83.85	62.00	64.90	56.80	37	5´ GTTTCTGCCTGCCTAGCAGTCATCATCACCTTCCCG 3´
								5´ GCGGGAAGGTGATGATGACTGCTAGGCAGGCAGAAAC 3´
C24AD27VT30A	4	81.57	85.59	68.90	72.30	64.60	48	5'GGCGTTTCTGCCGCCCTAGCAGTCATCATCGCCTTCCGCTGGACACC 3´
								5´ GGTGTCCAGCGGGAAGGCGATGATGACTGCTAGGGCGGCAGAAACGCC 3´
H145LH147L	2		82.26	63.10	66.00	59.50	37	5´ GCAAGCACAAAGCCTTCTGCTCGGGATCAAACCCCG 3´
								5´ GCGGGGTTTGATCCCGAGCAGAAGGCTTTGTGCTTGC 3´

Tab.2: Parameters of primers used in PCR-based site-directed mutagenesis (method „QuikChange“).
Parameter "T_m – williamstone" has been computed at www.williamstone.com
Parameter T_m – QuikChange has been derived from equation: $\mathbf{T_m = 81.5 + 0.41\ (\%GC) – 675/A - \%\ mismatch}$
Where A is the primer length in base pairs
Parameter T_m A has been derived from formula: $\mathbf{T_m\ (A) = 81.5 + 16.6\ (log[conc.of\ ions]) + 0.41\ (\%GC) – (600/length) – 0.63\ (\%\ phormamide)}$
Where conc. of ions = 60 mM; phormamide = 10%
Parameter T_mB has been derived from formula: $\mathbf{T_m(B) = 81.5 + 16.6\ (log\ [conc.K^+]) + 0.41\ (\%GC) – (675/length)}$
Where K^+ = 50 mM

3.3.3 PCR, reaction conditions

Site-directed mutagenesis is any of various techniques by which defined mutations can be made *in vitro* in a cloned DNA. It is widely used for studying protein structure – function relationship. Substitution of particular aminoacid(s) by another one and comparison of function of such altered protein with function of original ("wild") form can provide information of functional importance of each aminoacid. Impairment of function proofs for importance of substituted residue.

Stratagene´s kit QuikChange utilises *Pfu* DNA polymerase. Gene of interest is inserted into supercoiled double-stranded DNA vector. Two mutagenic primers – each antiparallel to opposite strand of mutated DNA – carry mutagenic mismatch. *Pfu* Turbo polymerase replicates both plasmid strands with high fidelity without displacing the mutant oligonucleotide primers. The oligonucleotide primers are extended during the temperature cycling. Incorporation of the oligonucleotide primers generates a mutated plasmid containing stagged nicks.

Next step following temperature cycling is the digestion of methylated and hemimethylated DNA (target sequence 5´-Gm6ATC-3´) with Dpn I endonuclease. As the parental DNA template originates from *Escherichia coli* it is dam methylated. Therefore parental strains are susceptible to Dpn I digestion and only newly synthetized strands carrying mutation are selected.

The nicked vector DNA incorporating the desired mutations is then transformed into *Escherichia coli* (Epicurian Coli XL-1 Blue supercompetent cells). Fig. 7.

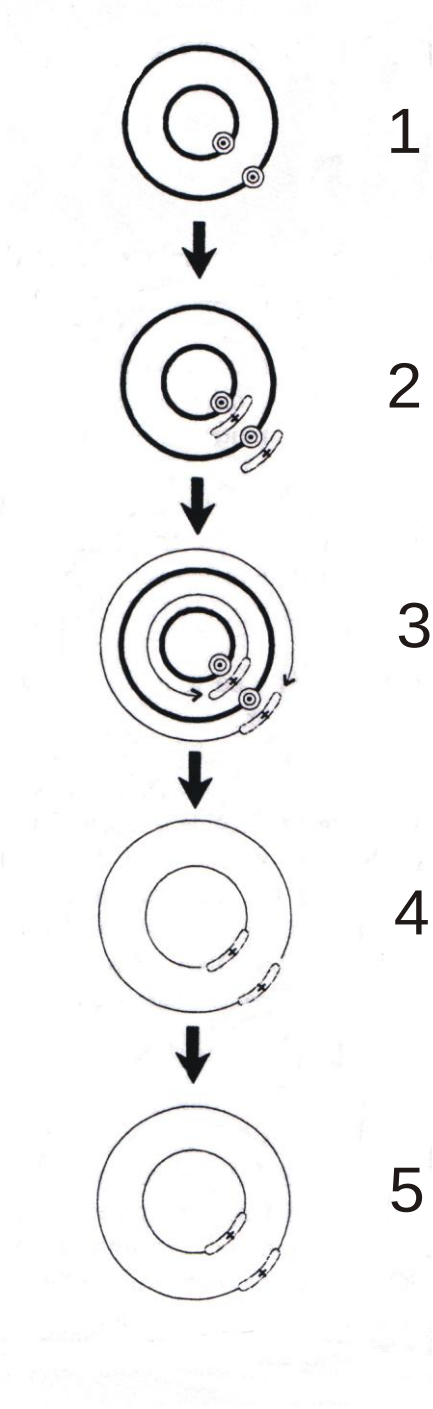

Fig. 7: Scheme of the PCR-based QuikChange site-directed mutagenesis
Step 1. Represents plasmid with UCP1 gene (spliced cDNA). The double circles mark places of desired mutation.
Step 2. Plasmid is denatured and two antiparallel primers – oligonucleotides possessing a mismatch with desired mutation(s) – are annealed.
Step 3. Nonstrand-displacing *Pfu Turbo* DNA polymerase synthesises new strands from mutagenic primers.
Step 4. Parental methylated nonmutated strands are displaced by *Dpn*I digestion.
Step 5. After transformation, supercompetent cells repair the nicks in the mutated plasmid.

3.3.3.1 Protocol:

Reaction mixture was prepared in thin wall micro-tubes. Tubes were placed on ice to prevent or minimize false priming.

5 µl of 10x Reaction Buffer (100 mM KCl, 60 mM $(NH_4)_2SO_4$, 200 mM Tris-HCl, pH 8., 20 mM $MgCl_2$, 1% Triton X-100, 100 µg/ml nuclease-free BSA
10 µl of plasmid DNA (~30 ng)
1.25 µl of oligonucleotide primer #1 (125 ng)
1.25 µl of oligonucleotide primer #2 (125 ng)
1 µl of dNTP mix
30.5 µl of sterile water
1 µl of *Pfu* polymerase (2.5 U)

Tubes were centrifuged shortly and 20 µl of mineral oil was overlaid onto the surface of the reaction mixture.
In cycler with temperature gradient tubes were placed in the way that each annealing-temperature parallels were in corresponding well of the block.
After first denaturation 20 cycles were run, composed of three steps:

1. 18 min. elongation at 68 °C
2. 30 s denaturation at 95 °C
3. 1 min. annealing

After temperature cycling the reaction was placed on ice for 2 min. to cool the reaction to the temperature below 37 °C.

1 µl of *Dpn* I restriction enzyme was added directly into the reaction (below the layer of mineral oil). Reaction was incubated at 37 °C for 1 hour .

3.3.4 Electrophoretic analysis

Electrophoresis in 0.8% agarose in 1 x TBE buffer (90 mM Tris base, 90 mM boric acid, 2 mM EDTA, pH 8.0) was performed in gel doped with EtBr. Total voltage 70 V for small gel or 150 V for large gel was set to reach relative value of 5V/cm. Gels were photodocumented. Fig. 8.

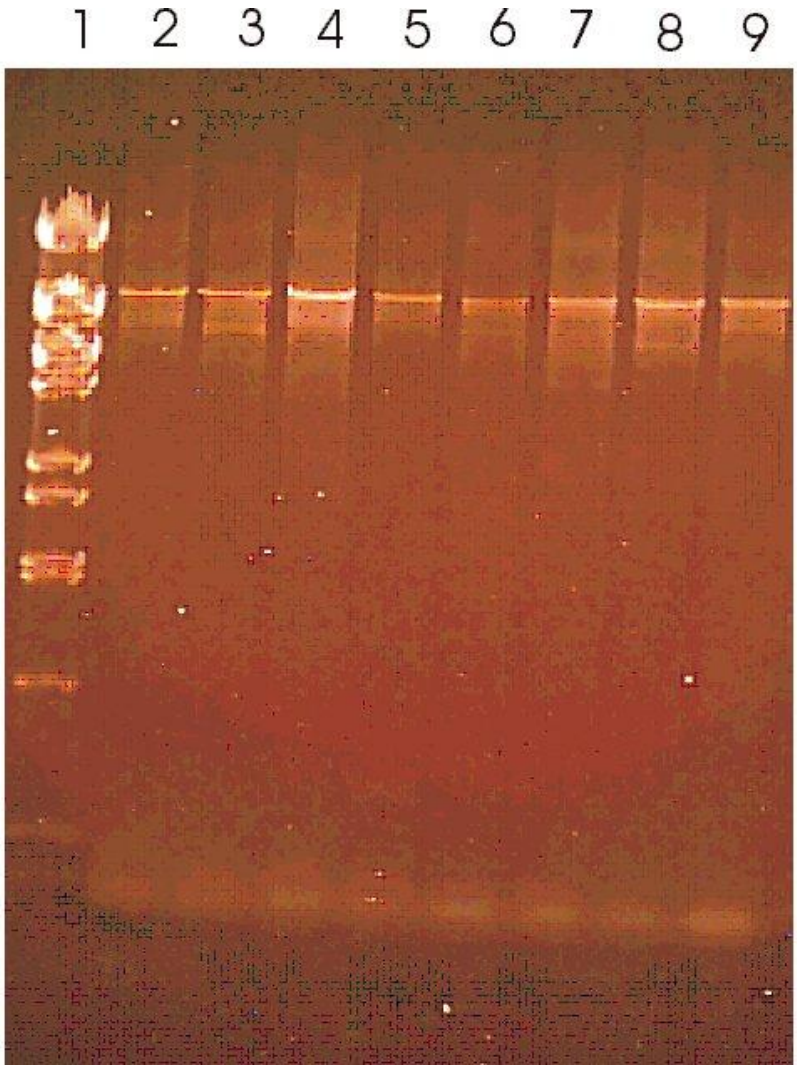

.

Fig.8: Agarose electrophoresis of mutagenic-PCR (20 cycles) amplicons run at gradient of annealing temperatures. Elongation was run at 68˚C for 18 min, denaturation at 95˚C for 30 s. Annealing lasted 1 min. Dependence of product amount on annealing temperature is visible.

Line1. Eco91I digested λ DNA, used as the standard
Line 2. Asp27Val UCP1 mutation, annealing temperature 46.1 ˚C, dilution of the template 1: 40
Line 3. Asp27Val UCP1 mutation, annealing temperature 57.1 ˚C, dilution of the template 1: 40
Line 4. Asp27Val UCP1 mutation, annealing temperature 65.1 ˚C, dilution of the template 1: 40
Line 5. Asp27Val UCP1 mutation, annealing temperature 57.1 ˚C, dilution of the template 1: 30
Line 6. H145LH147L UCP1 mutation, annealing temperature 46.1 ˚C, dilution of the template 1: 40
Line 7. H145LH147L UCP1 mutation, annealing temperature 57.1˚C, dilution of the template 1: 40
Line 8. H145LH147L UCP1 mutation, annealing temperature 65.1 ˚C, dilution of the template 1: 40
Line 9. H145LH147L UCP1 mutation, annealing temperature 57.1˚C, dilution of the template 1: 30

3.4 Transformation of bacteria, selection of positive clones

Escherichia coli (Epicurian Coli XL-1 Blue supercompetent cells) were used for transformation by amplified, *Dpn* I digested vector, carrying mutated UCP1 gene.

Bacteria were gently thawed on ice. 50 μl of these supercompetent cells were aliquoted into sterile prechilled 15 ml polypropylene tubes. From 2 to 10 μl of reaction was transferred into tubes with bacterial suspension. Reaction was mixed on Vortex and incubated for 30 min. on ice. 45 s lasting heat shock facilitating the transformation was done by submerging tubes into 42 °C preheated water bath for 45 s., followed by 2 min. exposition to ice temperature.

0.5 ml of LB medium supplemented with glucose to 0.02 M final concentration and with 12.5 mM $MgCl_2$ and 12.5 mM $MgSO_4$, preheated to 42 °C was added. Reaction was incubated at 37 °C for 1 h while shaking at 225 – 250 rpm. Then the reaction was spread onto LB – ampicillin (carbenicillin) plate and incubated at 37 °C overnight – two days. White colonies of successfully transformed bacterial clones were picked up and inoculated onto new plates.

3.4.1 Media, maintenance, selection

Escherichia coli (Epicurian Coli XL-1 Blue supercompetent cells) were propagated in 2 x YT (1.6 % bactotryptone, 1% yeast extract, 0.5 % NaCl, pH = 7.0) or LB (1% bactotryptone, 0.5 % yeast extract, 1% NaCl, pH = 7.0). Each of these media was supplemented by carbenicillin and/or ampicilin to final concentration 25 μl/ml.

In plates 1.5% bactoagar is the additional compound.

3.4.2 Propagation of bacteria

Escherichia coli (Epicurian Coli XL-1 Blue supercompetent cells) carrying vector with mutated UCP1 cDNA were propagated in 5 – 7 ml of LB or 2 x YT media with antibiotics at 37 °C overnight.

3.5 Plasmid DNA isolation

Isolation of shuttle vector pCGS110 was based on alkaline lysis followed by adsorption on anion exchange resin and high salt elution: at high pH and in presence of the detergent – SDS, the bacterial cell membranes and proteins are denatured. Upon neutralization, completely native

supercoiled plasmid molecules are reformed. The large size of chromosomal DNA (relative to the smaller supercoiled plasmid molecules) prevents renaturation, and it co-precipitates during neutralization. RNA binding to the exchange resin together with plasmid DNA was removed by RNAse digestion. The excessive salt was removed by gel filtration in spin column.

Commercial "ψ Clone plasmid preparation kit" from Princeton Separations, U.S.A. was used. Isolation procedure was done according to manufacturer´s instructions.

3.6 Sequencing

Primers for sequencing were designed as oligonucleotides antiparallel to sequence fragments of wild type UCP1 cDNA, with span shorter than 350 bp.
Alignment of sequenced UCP1 DNA with wild type UCP1 sequence, confirmation of QuikChange - implemented mutation and exclusion of clones carrying undesired spontaneous nucleotide substitutions was done by MegAlign software. Clones carrying desired mutation(s) surrounded by intact UCP1 sequence were selected for electroporation into yeast.

Sequencing was performed by using ALF Pharmacia sequencer. Method is based on T7 DNA Polymerase catalyzed synthesis of dideoxy nucleotide terminated chains. Reaction is run in four parallels, each corresponding to one of four (A,T,G,C) bases. In each reaction mixture one of four nucleotides is partially substituted by dideoxy analog.
Primers for sequencing were designed as oligonucleotides antiparallel to sequence fragments of wild type UCP1 cDNA with span shorter than 350 bp. To ensure best performance, primers were designed with GC rich 3´ ends. Primers were labeled by fluorescein – dATP in polymerase catalyzed reaction preceeding sequencing.
For best fluorescein - dATP labeling, condition, that first adenine of the sequence following 3´ end of the primer occupies one of first 3 – 4 positions, was fulfilled.
Template was denatured by NaOH, primers were annealed at 42 ˚C.
After four parallel sequencing reactions were completed, samples were denatured and electrophoresed on slab gels. When migrating through the gel, DNA fragments pass the fixed laser beam and generate fluorescent signal. Signals from four parallel lines corresponding to each of four bases are merged electronically into one graph. Fig. 9.

3.6.1 Computer analysis

Alignment of sequenced UCP1 DNA with wild type UCP1 sequence, confirmation of QuikChange - implemented mutation and exclusion of undesired spontaneous nucleotide substitutions was done by MegAlign software. Clones carrying desired mutation(s) and intact flanking UCP1 sequence were selected for electroporation into yeast. Fig. 9.

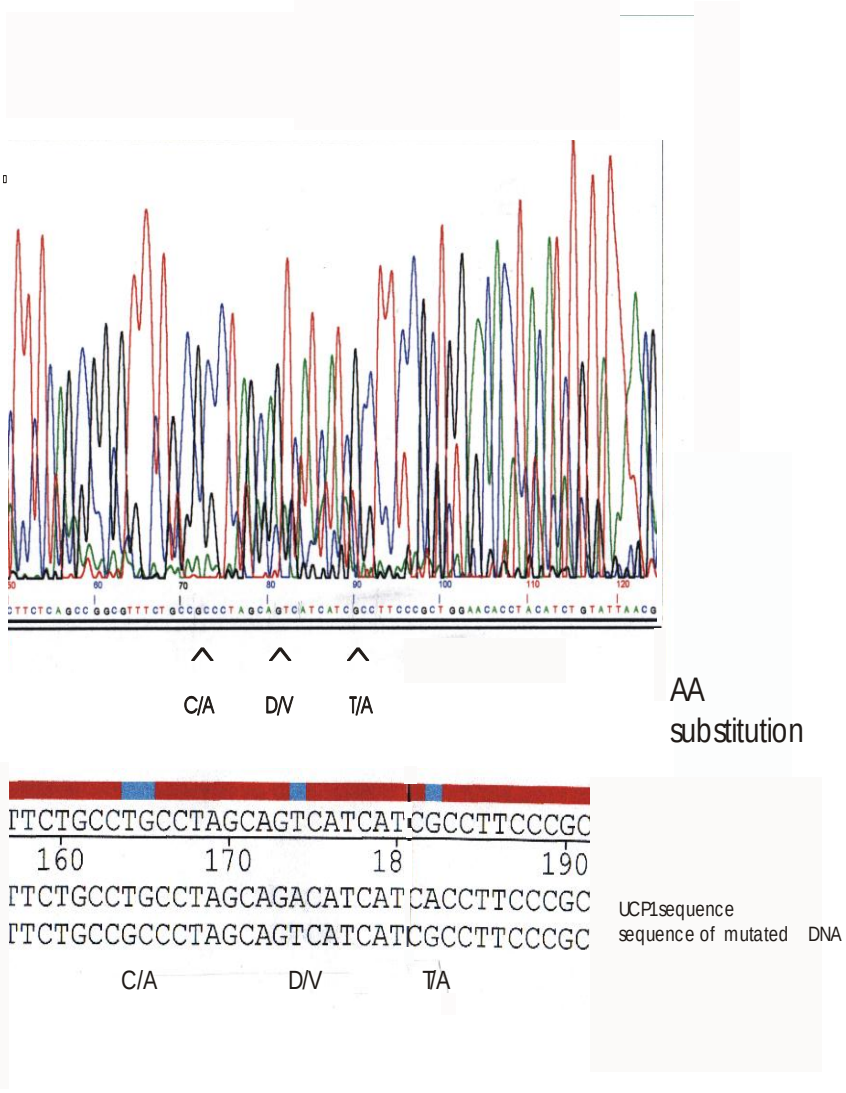

Fig. 9: Raw data from the sequence of UCP1 DNA fragment carrying triple AA substitutions and the alignment (MegAlign software) of this sequence with the wild type UCP1 DNA sequence.

3.7 Electroporation

3.7.1 Yeast strain

Yeast strain of *Saccharomyces cerevisiae* JB 516 – MAT*a ura3 ade1 leu2 his4 gal*$^{+}$ was used for electroporation

3.7.2 Electroporation

100 ml of YPD medium was inoculated with yeast strain JB 516. Culture was grown overnight. Yeast was centrifugation pelleted at 1000 g for 5 min. Yeast pellet was resuspended in 50 ml ice cold sterile water and centrifuged again. Then the pellet was resuspended in 10 ml of cold sterile water, centrifuged. The resulting pellet was resuspended in 2 ml of sterile ice cold 1 M sorbitol and pelleted by centrifugation. Finally yeast was resuspended in 300 μl of sorbitol.

Sterile electroporation cuvettes with 0.2 mm gap between electrodes were prechilled on ice. 40 μl of yeast suspension in sorbitol were mixed with 1 μl of DNA and transferred into electroporation cuvette. The cuvette was put into circuit of electroporator and electroporated by pulse of 2000 V (preset internal resistance of appliance 129 Ω). 960 μl of ice cold 1 M sorbitol was added immediately, solution was mixed well by cyclic pipetting and spread onto ura^{-} selective plates. Plates were incubated 2 – 4 days at 30 °C.

3.7.3 Selective media, maintenance

Yeast, carrying expression shuttle vector with particular mutated UCP1 cDNA, was proliferated on selective (ura^{-}) plates or in liquid ura^{-} media (0.17% YNB, 0.5% $(NH_4)_2SO_4$, 0.0005% each of adenine, L-leucine, L-histidine, L-tryptophan, L-methionine and L-arginine, 2% glucose, pH = 6.5). In plates 2% bactoagar is the additional compound.

Stock of each yeast strain or clone carrying vector with mutated UCP1 cDNA was stored at –70 °C in ura^{-} cultivation medium with 50% glycerol.

Stock of clones in use was in parallel way grown on plates with ura^{-} solid medium at 4 °C and passaged onto new plates every two months.

3.8 Expression

3.8.1 Galactose promotor

3.8.2 Expression media

Expression of rat UCP1 (cDNA derived) gene controlled by galactose promotor is stimulated in media with galactose: 0.17% YNB, 0.5% $(NH_4)_2SO_4$, 0.0005% each of adenine, L-leucine, L-histidine, L-tryptophan, L-methionine and L-arginine, 2% lactate and 0.05% glucose. pH = 6.5

Lactate serves as the main source of carbon in this media. Low concentration of glucose allows continuous switch of yeast metabolism from preferred carbon source - glucose to another one (lactate) at the beginning of cultivation in this medium.

Galactose to final concentration 0.2% was added to start UCP1 expression.

3.8.3 Conditions

Yeast culture from selective (ura^-) plates was inoculated into liquid ura^- media (0.17% YNB, 0.5% $(NH_4)_2SO_4$, 0.0005% each of adenine, L-leucine, L-histidine, L-tryptophan, L-methionine and L-arginine, 2% glucose, pH = 6.5) and cultivated while shaking 250 rpm at 30 °C overnight. Two parallels of 30 ml of the same media in 250 ml Erlenmayer flasks were inoculated by 2 ml of culture from previous day and cultivated at 30 °C overnight. Next day the culture was dissolved by fresh ura^- media into 4 – 5 30 ml parallels of the same media to the final $O.D_{600}$ = 0.3. Galactose was added to stimulate UCP1 expression. Cultivation lasted to $O.D_{600}$= 1.0 [90]

3.9 Isolation of mitochondria

Yeast culture grown to OD_{600} = 1 was collected and centifuged at 3000 g 5 min. Pellet was resuspended in 50 ml of 60 mM EDTA – NaOH, pH = 8.0; 1% merkaptoethanol and slowly stirred at 37 °C for 45 min. Then the culture was centrifuged again in preweighted cuvettes at the same conditions as in first centrifugation step. The supernatant was discarded and the weight of the pellet was established. Enzyme digesting yeast cell wall – Zymolyase was dissolved in spheroplasting buffer (1.2 M sorbitol, 20 mM Kpi, pH = 7.4) in ratio 1 mg of Zymolyase : 1 ml of spheroplasting buffer in amount: 1 mg of Zymolyase per 1 mg of wet weight of yeast. Inhibitor of

proteases PMSF was added (10 μl per 1 ml of complete buffer). Pellet was resuspended in this buffer and incubated at mild shaking at 30 °C for 30 min.

Destruction of yeast cell wall was checked in microscope at 45x magnification. 3 μl of solution with Zymolyase treated yeast were dissolved in two parallels in 20 μl of sorbitol (negative control – isotonic environment in which spheroplasts keep circular shape) and in 20 μl of water. Rupture of cells in parallel with water must be visible.

Solution of yeast with digested cell wall is transferred into new centrifugation tubes and centrifuged at 2000 g for 5 min. Pellet is resuspended in 15 ml of 1.2 M sorbitol and again centrifuged at 2000 g for 5 min. This step is repeated one more time. Pellet was resuspended in 7 ml of breaking buffer (0.6 M sucrose, 20 mM HEPES-KOH, 1 mM PMSF, 0.1 % BSA, pH = 6.5) and homogenized in glass homogenizer. The resulting homogenate was centrifuged at 700 g for 5 min. The turbid supernatant was transferred into new centrifugation tube and centrifuged at 9800 g for 10 min. Pellet was resuspended in 5 ml of breaking buffer without BSA (0.6 M sucrose, 20 mM HEPES-KOH, 1 mM PMSF, pH = 6.5) and again centrifuged at 9800 g for 10 min. The supernatant was discarded and pellet was resuspended in 0.5 ml of breaking buffer.

3.10 Western blot analysis

3.10.1 ELPHO

Discontinuous modification (Laemmli system) of sodium dodecylsulfate (SDS) electrophoresis in polyacrylamide gel (PAGE) was used for the detection of UCP1 proteins.

Anionic detergent SDS denatures proteins by wrapping around their polypeptide backbone. Hence, the charge of the molecule is proportional to the length of the molecule. Reducing agent (2-mercaptoethanol) acts to homogenize the negative charge along the whole molecule. Separation according to the molecular weight is thus performed.

In discontinuous SDS – PAGE two gels are used: stacking gel with relatively low density and separating gel. During their way, proteins concentrate in the border zone between these gels so that the resolution in the separating gel is much better than in setup with only one gel.

Separation and molecular weight-based detection of expressed and isolated UCP1 mutated proteins (molecular weight ~ 32 000) was performed in 1 mm thick gels in Hoeffer Sci. appliance MIGHTY SMALL SE 250. Density of stacking gel was 3.7%; density of separation gel was 12%. Mixtures of proteins of defined molecular weight – Full Range Rainbow from Amersham and Prestained SDS-PAGE Standards, Low Range from Bio-Rad were used for calibration.

3.10.2 Blotting, development

Separated UCP1 proteins were blotted onto nitrocellulose membrane (BIO-RAD, thickness 0.45 μm) 8 x 5.5 cm in appliance TE-22 in trans blot buffer (20 mM TRIS-HCl, 500 mM NaCl, pH = 7.5) at electric current 120 mA for 45 min. Nonspecific binding was prevented by saturation of the membrane by protein (3% solubilized non-fat milk in trans blot buffer) for 60 min. Membrane was washed three times in trans blot buffer with 0.05% Tween – 20. Membrane was exposed to primary anti-rat UCP1 antibody (polyclonal rabbit anti-UCP1, kind gift of Garlid´s group) for 1 – 1.5 hour and three times washed in trans blot buffer with 0.05% Tween – 20 as in previous step. Incubation in secondary antibody – goat anti rabbit alkaline phosphatase conjugate (Sigma, cat. No. A8025, goat anti-whole molecule of rabbit Ig) diluted 1 : 5 000. After 3- time washing in trans blot buffer, bound secondary antibody was detected. BCIP/NBT solution was used as substrate.

3.11 Total protein assessment

Amount of total proteins from isolated mitochondria was established by Lowry´s method based on Foline phenol reagent.
Samples were reacted with solution of 0.02% $CuSO_4$, 0.04% potassium tartarate, 2% Na_2CO_3 and 0.1 M NaOH. After 15 min samples were treated with Folin reagent in final 24-fold dilution for another 15 min. Absorbance at 700 nm was measured and compared with calibration standards [108].

3.12 Preparation of proteoliposomes

The detergent, octypentaoxyethylene, was used to extract membrane proteins. The lipid mixture consisted of L-α-phosphatidylcholine, Sigma type XI, supplemeneted with 4.2% bovine heart cardiolipin and 1.6% L-α-phosphatidic acid. Two doses of lipids (I. - 27.5 mg and II. - 13.7 mg) were dried under nitrogen stream, dissolved in ether, redried and stored overnight under vacuum.
Lipids were solubilized in extraction medium (5 mM TEA-TES, 0.6 mM TEA-EGTA, 50 mM TEA_2SO_4) with 13 % octypentaoxyethylene. Dose I. of lipid mixture was added to mitochondria

and the reaction was stirred at 0˚C for 10 minutes. The mixture was then transferred onto polyethylene syringes, sealed with silicon fibres in the outlet, filled with 2 ml of wet hydroxylapatite and incubated 10 minutes at 20 ˚C and 30 minutes at 4 ˚C. Wet hydroxyapatite was prepared from 0.3 g of dry hydroxylapatite that had been incubated with extraction medium. The volume of eluate was established.

After incubation, solution in extraction medium was eluted by centrifugation. This hydroxylapatite eluate was mixed with another lipid dose II. of lipids and its final composition was set in case of Cl^- transport measurements: 12.8 mM TEA-Pi, 0.6 mM TEA-EGTA, 143.5 mM TEA_2-SO_4, pH = 7.2 in case of H^+ transport measurements: 28.85 mM TEA-TES, 0.6 mM TEA-EGTA, 84.4 mM TEA_2-SO_4, pH = 7.2. SPQ fluorescent probe was added to final 2 mM concentration. To remove detergent and form proteoliposomes, the lipid protein mixture was incubated at 4 ˚C overnight in syringes filled with Bio-Beads SM2 (Bio-Rad), prewashed and adjusted in internal media (12.8 mM TEA-Pi, 0.6 mM TEA-EGTA, 143.5 mM TEA_2-SO_4, pH = 7.2, for Cl^- uptake; 28.85 mM TEA-TES, 0.6 mM TEA-EGTA, 84.4 mM TEA_2-SO_4, pH = 7.2, for H^+ efflux). Next day solution with formed liposomes was eluted by centrifugation and transferred onto another column of the same composition for removal of remaining detergent. After 10 minute incubation at 4 ˚C, centrifugation - elution was done. External probe was then removed by passing proteoliposomes through Sephadex G-25-300 (Sigma) that had been preequilibrated with proper internal medium (4 g of Sephadex per one liposome preparation are weighted).

3.13 Measurement of transport

Transport function of UCP1 mutants was measured in UCP-liposomes loaded with fluorescent indicator compound 6-methoxy-N-(3-sulfopropyl)quinolinium (SPQ). This probe detects Cl^- ionts. In combination with TEA-TES (TES anion respectively) also H^+ transport can be detected in indirect way.

3.13.1 6-methoxy-N-(3-sulfopropyl)quinolinium (SPQ)*

UV radiation - excitated fluorescence of SPQ inside proteoliposomes is quenched by transient interaction between SPQ and Cl^- (halide anion generally) or TES anion. No ground state complex is formed during this interaction. In the case of this probe, quenching is not accompanied by spectral shifts. The efficiency of collisional quenching is characterized by the Stern-Volmer constant – the reciprocal of the ion concentration that produces 50% of maximum quenching. For SPQ Stern – Volmer constant is reported to be 118 M^{-1} in aqueous solution.

* Besides application in UCP1 functional studies, SPQ probe is used for the detection of intracellular Cl^- concentration in connection with function of chloride transport channel known as cystic fibrosis transmembrane conductance regulator; for measurement of Cl^- fluxes through transporters such as GABA receptor and erythrocyte Cl^-/HCO_3^- exchangers.

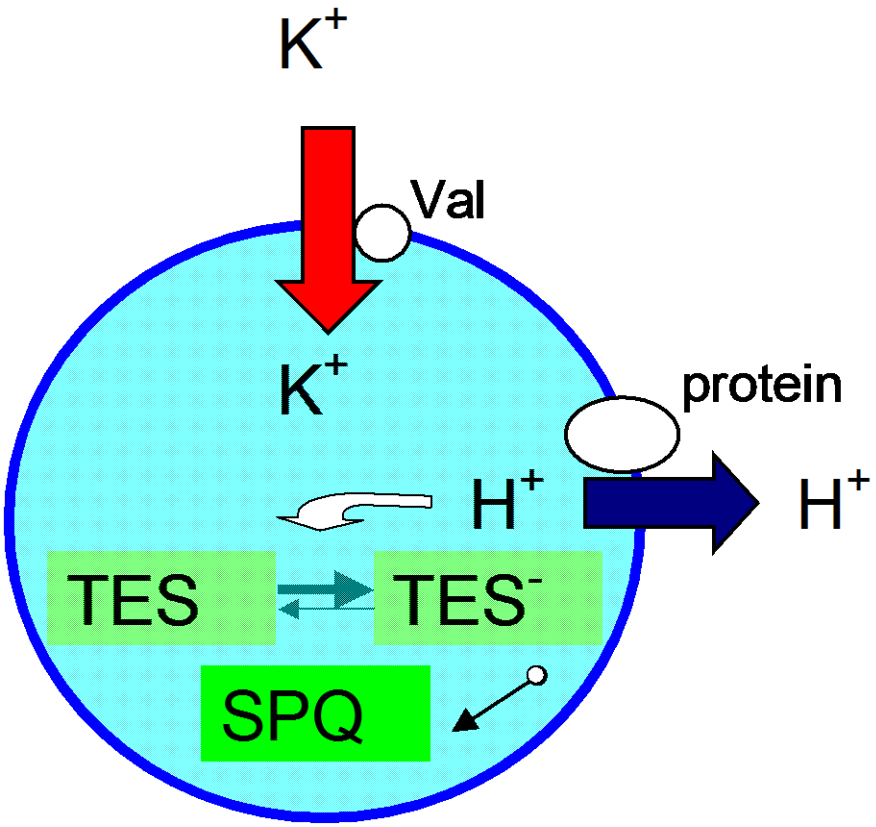

Fig. 10: Scheme of mechanism of H^+ measurement in proteoliposomes with trapped fluorescence probe SPQ. TES^- anion quenches SPQ fluorescence. H^+ concentration shifts the poise between TES^- anion and neutral TES zwitterion. Valinomycin serves as selective ionophore for K^+. K^+ migrates into liposomes according to concentration gradient causing change of electrochemical potential. This change drives H^+ efflux catalyzed by UCP1.

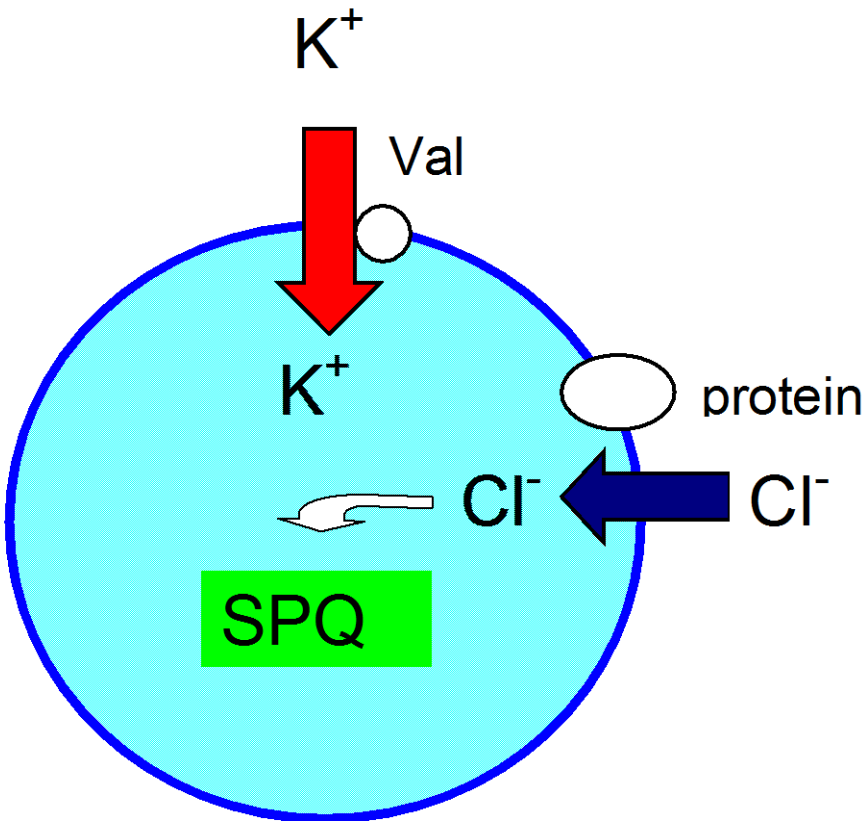

Fig. 11: Scheme of mechanism of Cl^- uptake measurement in proteoliposomes with trapped fluorescence probe SPQ. Cl^- anion quenches SPQ fluorescence. Valinomycin serves as selective protonophore for K^+. K^+ migrates into liposomes according to concentration gradient causing change of electrochemical potential. This change drives Cl^- uptake catalyzed by UCP1.

3.13.2 Fluorescence measurement of Cl^- uptake and H^+ efflux in proteoliposomes containing UCP1

Fluorescence of SPQ-loaded proteoliposomes was measured with an RF-5301PC spectrofluorometer (Shimadzu) controlled by original software run in Windows 98 environment. Excitation was set at 340 nm with a slit width of 10 nm, and emission at 444 nm with a slit width of 5 nm. Data acquisition rate was 0.3 s, number of readings 800. 25 µl of proteoliposome suspension was transferred to cuvette containing 1. 975 ml of external medium (28.85 mM TEA-TES, 0.6 mM TEA-EGTA, 84.4 K_2SO_4, pH = 7.2 for H^+ efflux; 12.8 mM TEA-Pi, 0.6 mM TEA-EGTA, 215 mM KCl , pH = 7.2 for Cl^- uptake).

Each proteoliposome preparation was calibrated to obtain the corresponding Stern-Volmer quench constant. The volume of the liposomes was estimated from the probe distribution [83,109].

H^+ efflux was promoted by addition of valinomycin (0.1 µM final concentration) at 20 s. The decrease of fluorescence indicates H^+ efflux, since SPQ fluorescence is quenched by TES^- anion. H^+ concentration is interrelated with poise between TES zwitterion and TES^- anion. Fig. 10., Fig. 12.

Cl^- uptake was promoted by addition of valinomycin (1 µM final concentration). Decrease of fluorescence indicates Cl^- uptake, since fluorescence of SPQ is quenched by Cl^-. Fig. 11.

At the end of each run a mixture of nigericin and tributyltin chloride (0.5 and 5 µl respectively) was added to equilibrate ion gradients [109].

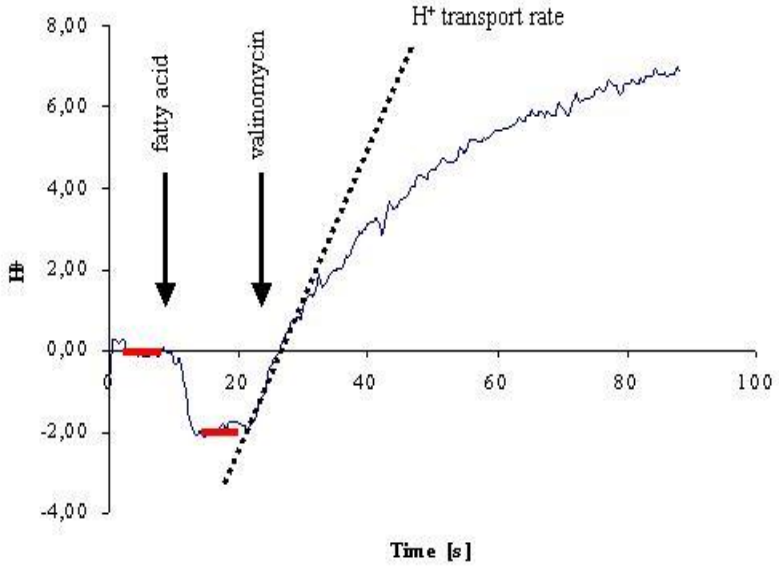

Fig. 12: The example of typical run of H^+ efflux. After the addition of fatty acid, the internal acidifacion causes drop of H^+ concentration. After addition of K^+ ionophore valinomycin, transport mediated by UCP1 starts.

3.14 Computation

For calculation of transport rates equation $F_0/F = 1 + K_q[Q]$ is used, where F and F_0 are fluorescence intensities observed in the presence and absence of quencher. [Q] is the concentration of quenching agent and K_q is the Stern-Volmer constant.

4 Results

4.1 Phylogenetic relations of newly annotated UCPs

Search for homologies in available genome databases revealed on the level of genes new members of UCP family. Employment of previously proposed conserved AA motifs [23] confirmed and rafined relations of these new members to another ones.

Four UCP sequences were found in *Drosophila melanogaster*, one in nematode *Caenorhabditis elegans*, one in model organism - soil amoeba belonging to Protists (*Protista*), but formerly ascribed to Fungi: *Dictyostelium discoideum* and one new UCP in plant *Arabidopsis thaliana*.

D. melanogaster sequence AE003506 (accession number in GADFly CG6492) clustered as the closest protein to human UCP4 (52.3% homology) in a constructed homology-based phylogenetic tree of all 43 MACP members found in *Drosophila* together with human MACP carriers of known phenotype and all five human UCPs, potato PUMP, two other *Arabidopsis* PUMPs and all known yeast MACPs. In a cluster together with the pair of AE003506 and human UCP4, another pair of *Drosophila* MACPs was located - AE003487 (GADFly CG 18340) and AE003612 (GADFly CG9064). The closest to this quarter was a pair of human BMCP and *Drosophila* AE003544 (GADFly CG7314, 50.8% homology to BMCP). These six proteins formed together one of the two branches of the most likely uncoupling protein subfamily, while the other branch contained UCP1, UCP2, UCP3 and PUMPs.

All these *Drosophila* proteins contain all α-helical UCP signatures in somewhat general form as well as the PNBD motif defined previously by Bouillaud et al., that also required an extended definition [88].

Both, the phylogenetic tree as well as UCP signature analysis ascribe the CG6492 protein (AE003506) as the *Drosophila* UCP4 analog (thereafter termed DmUCP4A). Fig. 13., Fig. 14. Also characters of UCP signatures in CG18340 (AE003487) and CG9064 suggest that these proteins are the closest UCP4 relatives - hereafter termed DmUCP4B and DmUCP4C. DmUCP4C represents a transition between the UCP4 and BMCP. All these *Drosophila* proteins could function as uncoupling proteins, since they are the closest UCP4 (or BMCP) relatives among all *Drosophila* MACPs.

In nematode *Caenorhabditis elegans* a protein AF 003384 (from a cosmid clone K07B1) is 44.3% homologous to human UCP4. It contains all three α-helical UCP signatures and PNBD with all UCP4 features plus BMCP-like feature in the first α-helical UCP signature and RYTG sequence (the same as in hUCP1) as a part of the second matrix UCP signature. The positive charge (lysine) is three residues apart from another one (arginine), not two as in human UCP4. Its PNBD motif contains a pair of negative charges (aspartates), exceptional among UCPs.

In the genome of *Dictyostelium discoideum* another predicted uncoupling-like protein was found. Its DNA fragments were composed of clones JAX4a7407.1 and II-CAP1D15012. Unfortunately the sequence is still incomplete. This protein contains mixed features of human UCP4 and BMCP (35.6% homology to both of them). It contains the BMCP-specific proline in the fourth α-helical UCP signature, but like UCP4 it contains nearly the whole second matrix UCP signature (with exceptional serine at the sixth position after the central positive charge). This protein was ascribed to UCP4 cluster. However, the phylogenetic tree placed this protein as separate branch of BMCP cluster. Fig. 13.

In *Arabidopsis thaliana* genome database a novel sequence belonging to UCP family was found: AC007576_24 (or F7A19_22) contains features characteristic for human UCP4 and is rather distant from *At*PUMP1 and *At*PUMP2 and from potato and *Symplocarpus* PUMPs. As in UCP4 the last residue of the first α-helical UCP signature is phenylalanine, the residue following arginine in the second α-helical UCP signature is histidine and three residues further there is threonine. It also contains a PNBD motif of the UCP4 type. This protein clusters with other UCP4 in phylogenetic trees. Fig. 13.

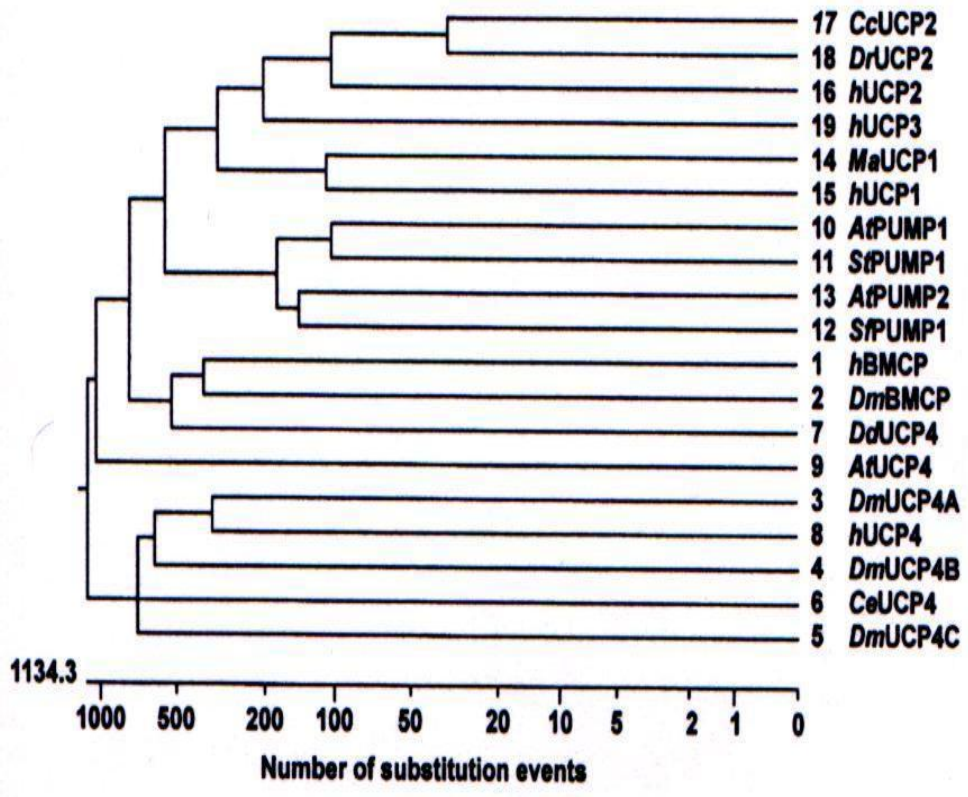

Fig. 13: Phylogenetic tree of predicted uncoupling proteins found in *Drososphila melanogaster*, *Caenorhabditis elegans*, *Dictyostelium discoideum* and *Arabidopsis thaliana* together with known human and fish UCPs and two other PUMPs. The phylogenetic tree documents two distinct branches of UCPs, a „UCP4 group“ and the group of all other UCPs. BMCPs form distinct subgroup (together with *Dd*UCP4) within the later group, closest to the UCP4 group.

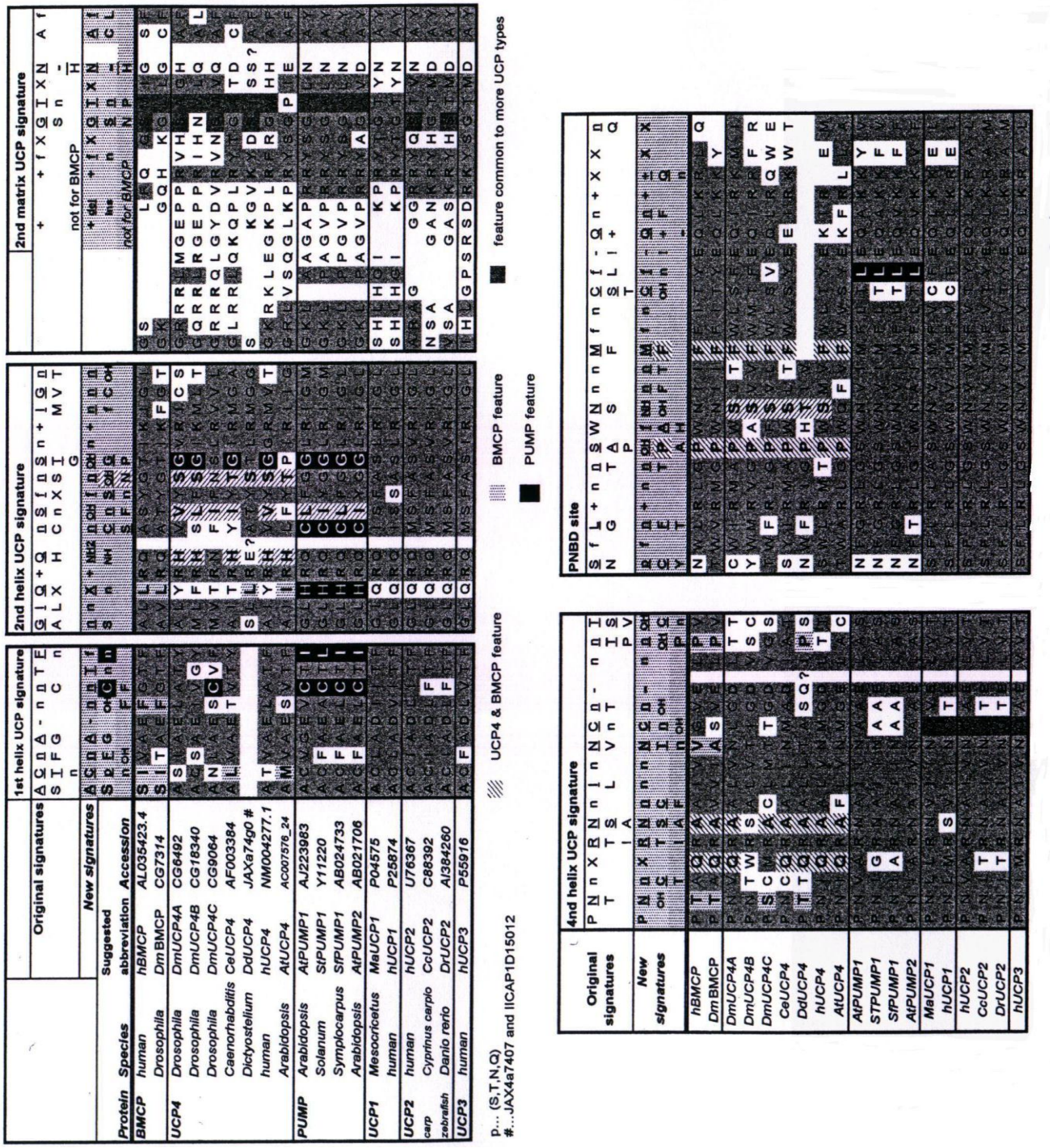

Fig.14: Analysis of UCP signatures and PNBD motifs in predicted uncoupling proteins of *D. melanogaster*, *C. elegans*, *D. discoideum* and *A. thaliana*. The UCP-specific sequence ('signature' for all UCPs but BMCP) in the second matrix segment is shown with preceding residues to illustrate distribution of positive charges in this segment. BMCP-specific features are indicated by the dotted background; PUMP-specific features by white fonts in the black background; UCP4-specific features by 45° hatching and UCP4 and BMCP common features by 135° hatching. The gray background represents features common to more UCPs. Question marks indicate irregularities in UCP signatures of the predicted *D. discoideum* UCP4. Symbols represent the following items: n, neutral non-aromatic residue including M; f, aromatic residue ; '+' or '-', positive or negative charged residues, respectively; OH stands for S or T; NH stands for N or Q; and, p represents S, T, N and Q. Stars depict the residues well conserved in the MACP family members (up to 10 exceptions); exclamation marks refer to the 'quite conserved' residues. The trans-membrane regions are depicted according to (Klingenberg 1990).

4.2 Substitutional mutants of rat UCP1

By the sequence of molecular biology techniques and heterologous expression in yeast, mutated species of rat UCP1 were obtained, containing substitutions of residues in 1st transmembrane α-helix C24, D27 and T30 and species containing mutations in 2nd matrix domain with substituted residues H145, H147 and R152. Fig. 15, Fig. 16.

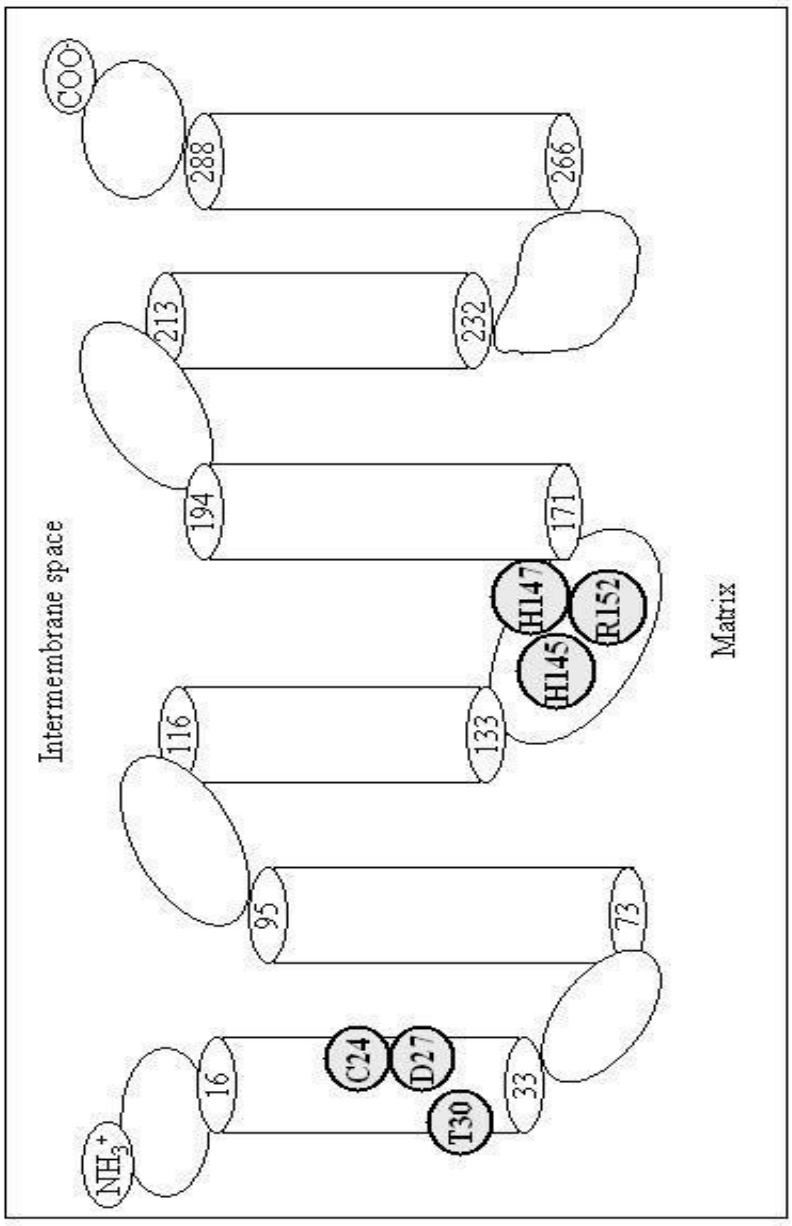

Fig. 15: The model of transmembrane spanning of UCP1 is drawn with indicated AARs mutated (small elipse). The transmembrane segments are represented by cylinders. AARs at the interface of the membrane are indicated by their sequence position numbers.

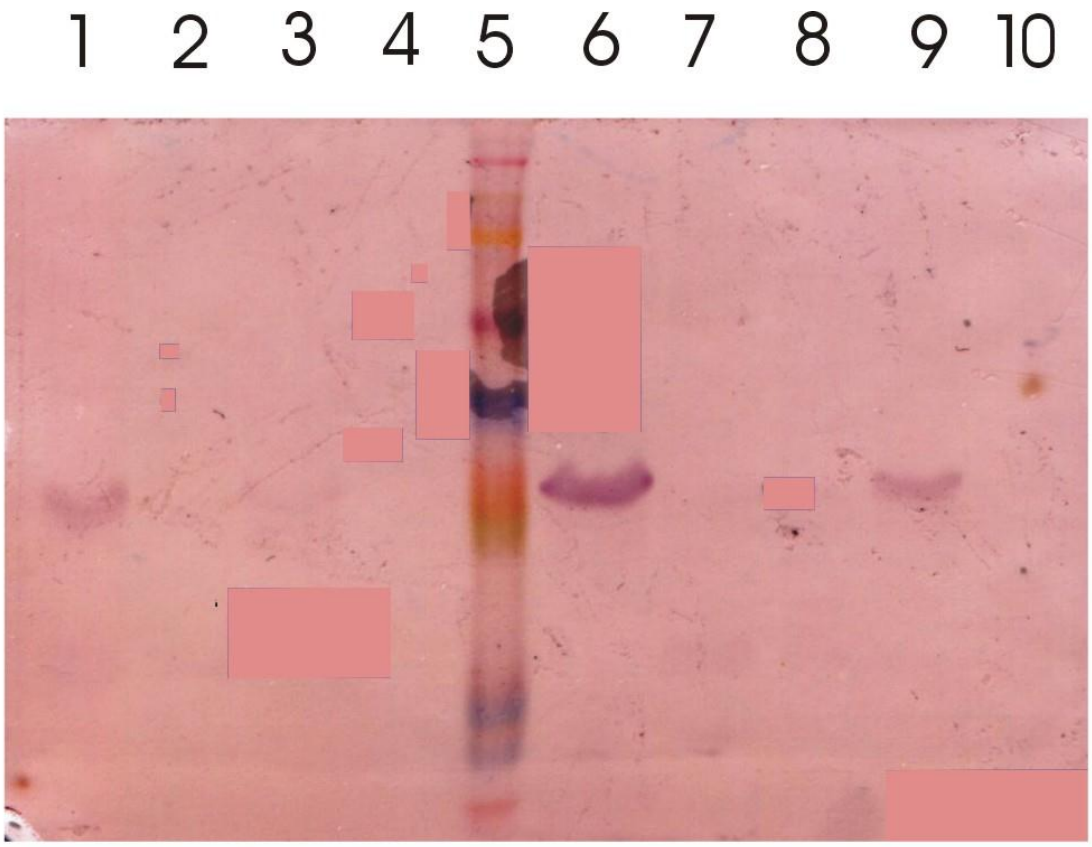

Fig. 16: Western blot of UCP1 mutants expression in yeast.
Line 1. UCP1 mutant Thr30Ala expressed in medium with galactose
Line 2. UCP1 mutant Thr30Ala expressed in medium without galactose
Line 3. UCP1 mutant Asp27Val expressed in medium with galactose
Line 4. UCP1 mutant Asp27Val expressed in medium without galactose
Line 5. Molecular weight standard. Orange color represents molecular weight 30 000, blue color represents 35 000.
Line 6. UCP1 mutant H145LH147L expressed in medium with galactose
Line 7. UCP1 mutant H145LH147L expressed in medium without galactose
Line 8. UCP1 mutant Lys72Glu used as positive control
Line 9. UCP1 mutant C24AD27VT30A expressed in medium with galactose
Line 10. UCP1 mutant C24AD27VT30A expressed in medium without galactose

4.2.1 WT

The values of proton transport in the presence of 100 μM lauric acid are 58 ± 23 μmol $H^+min^{-1}mg^{-1}$; 54 ± 17 μmol $H^+min^{-1}mg^{-1}$ in the presence of 75 μM lauric acid and 49 ± 15.8 μmol $H^+min^{-1}mg^{-1}$ in the presence of 50 μM lauric acid. Fig. 21, Fig 25 (both expressed as turnover number).

Maximal transport rate (V_{max} – Lineweaver-Burk) for proton transport was 104.56 μmol $H^+min^{-1}mg^{-1}$. Value of Michaelis-Menten constant (K_m - Lineweaver-Burk) was 76.8 μM. Fig. 23, Fig. 24.

Data from linear regression of H^+ transport as a function of UCP1 concentration, at different concentrations of lauric acid: Maximal transport rate (V_{max} – Lineweaver-Burk) for proton transport was 18.5 μmol $H^+min^{-1}mg^{-1}$. Value of Michaelis-Menten constant (K_m - Lineweaver-Burk) was 44.6 μM. Fig. 22, Fig. 26.

The values of proton transport at extrapolation of lauric acid concentration to 100 μM: 13.454 μmol $H^+min^{-1}mg^{-1}$. Fig. 26.

4.2.2 C24AD27VT30A

The values of proton transport in the presence of 100 μM lauric acid are 5.8 ± 1.1 μmol $H^+min^{-1}mg^{-1}$ (**10%** of wt); 4.15 ± 0.2 μmol $H^+min^{-1}mg^{-1}$ in the presence of 75 μM lauric acid and 3.3 ± 0.4 μmol $H^+min^{-1}mg^{-1}$ in the presence of 50 μM lauric acid. Fig. 21, Fig. 25 (both expressed as turnover number).

Maximal transport rate (V_{max} – Lineweaver-Burk) for proton transport was 11.6 μmol $H^+min^{-1}mg^{-1}$ i.e. **11.1%** of the wt. Value of Michaelis-Menten constant (K_m - Lineweaver-Burk) was 94.8 μM. Fig.17, Fig. 23, Fig. 24.

Data from linear regression of H^+ transport as a function of UCP1 concentration, at different concentrations of lauric acid: Maximal transport rate (V_{max} – Lineweaver-Burk) for proton

transport was -1.5 μmol $H^+min^{-1}mg^{-1}$ i. e. **0.0%** of the wt. Value of Michaelis-Menten constant (K_m - Lineweaver-Burk) was 281.5 μM. Fig. 22, Fig. 26.

The values of proton transport at extrapolation of lauric acid concentration to 100 μM: -0.339 μmol $H^+min^{-1}mg^{-1}$ (**0.0%** of wt). Fig. 26.

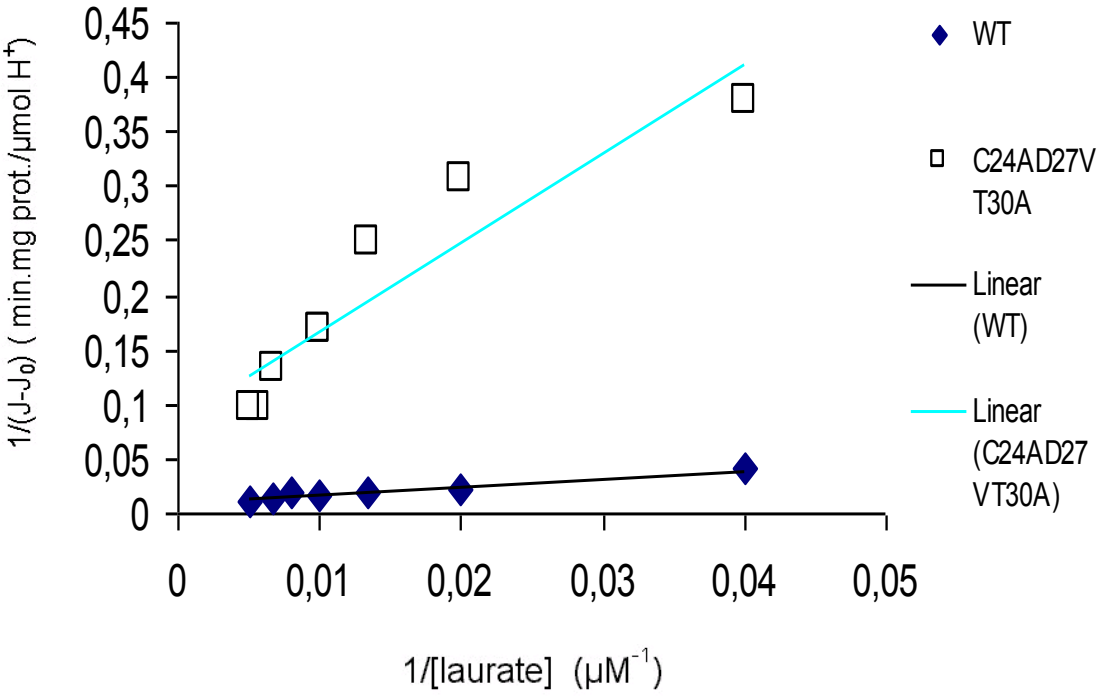

Fig. 17: The comparison of lauric acid activated - proton efflux kinetics of UCP1 wt and UCP1 C24AD27VT30A mutant is shown as double reciprocal (Lineweaver – Burk) plot. The flux J_0, caused by valinomycin in the absence of lauric acid, was subtracted.

4.2.3 D27V

The values of proton transport in the presence of 100 μM lauric acid are 14.5 ± 1.4 μmol $H^+min^{-1}mg^{-1}$ (**25%** of wt) ; 13.1 ± 0.16 μmol $H^+min^{-1}mg^{-1}$ in the presence of 75 μM lauric acid and 14.9 ± 6.8 μmol $H^+min^{-1}mg^{-1}$ in the presence of 50 μM lauric acid. Fig. 21, Fig. 25 (both expressed as turnover number).

Maximal transport rate (V_{max} – Lineweaver-Burk) for proton transport was 61.7 μmol $H^+min^{-1}mg^{-1}$ i.e. **59%** of the w.t. Value of Michaelis-Menten constant (K_m - Lineweaver-Burk) was 244.5 μM. Fig. 18, Fig. 23, Fig. 24.

Data from linear regression of H^+ transport as a function of UCP1 concentration, at different concentrations of lauric acid: Maximal transport rate (V_{max} – Lineweaver-Burk) for proton transport was 14.1 μmol $H^+min^{-1}mg^{-1}$ i. e. **76.2%** of the wt. Value of Michaelis-Menten constant (K_m - Lineweaver-Burk) was 242.6 μM. Fig. 22, Fig. 26.
The values of proton transport at extrapolation of lauric acid concentration to 100 μM: 4.037 μmol $H^+min^{-1}mg^{-1}$ (**30%** of wt). Fig. 26.

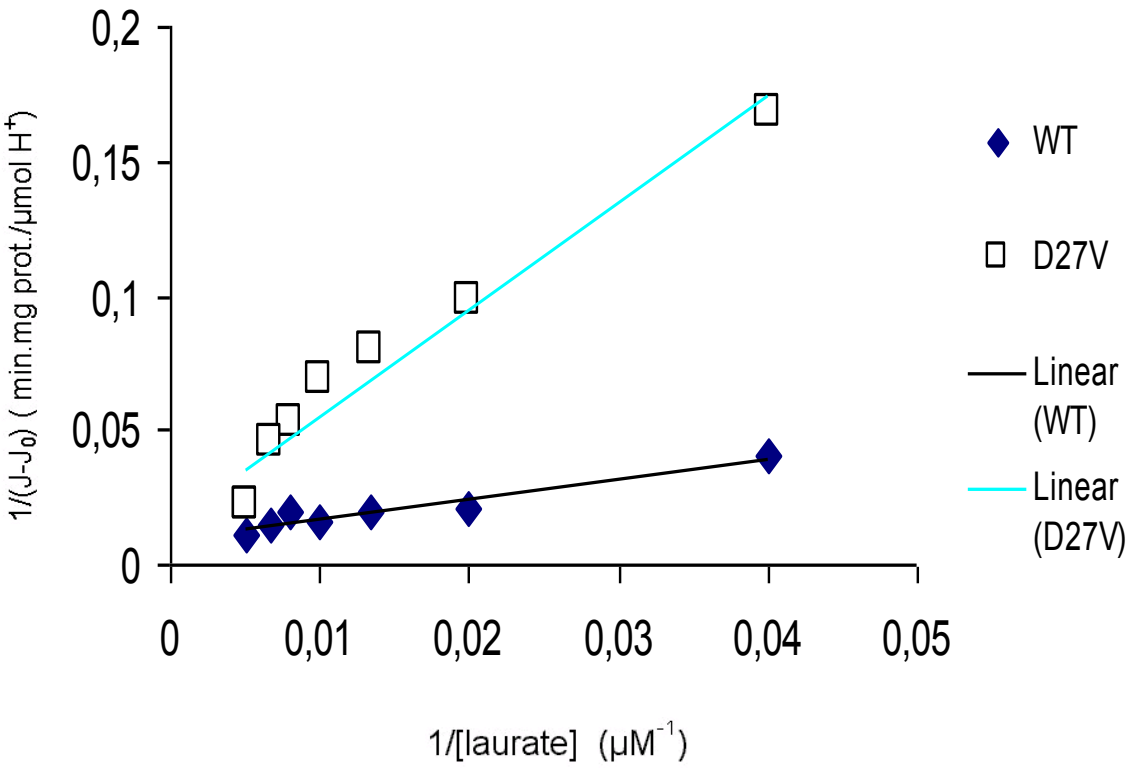

Fig. 18: The comparison of lauric acid activated - proton efflux kinetics of UCP1 wt and UCP1 D27V mutant is shown as double reciprocal (Lineweaver – Burk) plot. The flux J_0, caused by valinomycin in the absence of lauric acid, was subtracted.

4.2.4 T30A*

The values of proton transport in the presence of 100 μM lauric acid are 22 ± 6 μmol $H^+min^{-1}mg^{-1}$ (**37.9%** of wt); 21.4 ± 6.8 μmol $H^+min^{-1}mg^{-1}$ in the presence of 75 μM lauric acid and 17.1 ± 1.6 μmol $H^+min^{-1}mg^{-1}$ in the presence of 50 μM lauric acid. Fig. 21, Fig. 25 (both expressed as turnover number).

Maximal transport rate (V_{max} – Lineweaver-Burk) for proton transport was 72.9 μmol $H^+min^{-1}mg^{-1}$ i.e. **69.7%** of the wt.. Value of Michaelis-Menten constant (K_m - Lineweaver-Burk) was 160.2 μM. Fig. 19.

* Proton transport data of this mutant presented in this dissertation do not correspond to values presented in article 110. Author of this dissertation can guarantee just the data presented here, irrespectively of the fact, that data in the article are based on much more extensive set of measurements so that should characterize the mutant in more objective way. Further measurements would be beneficial to confirm H^+ transport characteristics of T30A UCP1.

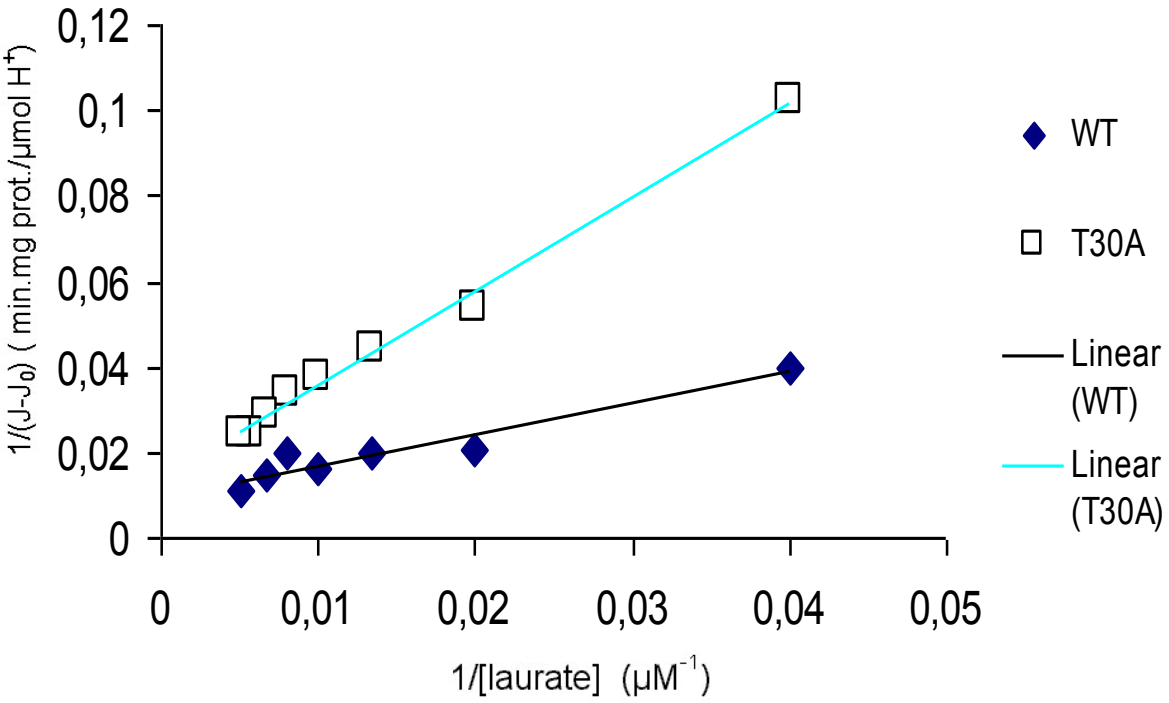

Fig.19: The comparison of proton efflux activated by lauric acid kinetics of UCP1 wt and UCP1 T30A mutant is shown as double reciprocal (Lineweaver – Burk) plot. The flux J_0, caused by valinomycin in the absence of lauric acid, was subtracted.

4.2.5 H145LH147L

The values of proton transport in the presence of 100 μM lauric acid are 13.9 ± 11.5 μmol $H^+min^{-1}mg^{-1}$ (**23.9%** of the wt) ; 6.7 ± 4.3 μmol $H^+min^{-1}mg^{-1}$ in the presence of 75 μM lauric acid and 4.9 ± 3.3 μmol $H^+min^{-1}mg^{-1}$ in the presence of 50 μM lauric acid. Fig. 21, Fig. 25 (both expressed as turnover number).

Data from linear regression of H^+ transport as a function of UCP1 concentration, at different concentrations of lauric acid: Maximal transport rate (V_{max} – Lineweaver-Burk) for proton transport was 4.5 μmol $H^+min^{-1}mg^{-1}$ i. e. **24.3%** of the wt. Value of Michaelis-Menten constant (K_m - Lineweaver-Burk) was 57.0 μM.
The values of proton transport at extrapolation of lauric acid concentration to 100 μM: 3.305 μmol $H^+min^{-1}mg^{-1}$ (**24.5%** of wt). Fig. 26.

4.2.6 R152L

The values of proton transport in the presence of 100 μM lauric acid are 32.6 ± 21.4 μmol $H^+min^{-1}mg^{-1}$ (**56.2%** of the wt); 24.4 ± 13.0 μmol $H^+min^{-1}mg^{-1}$ in the presence of 75 μM lauric acid and 25.0 ± 14.8 μmol $H^+min^{-1}mg^{-1}$ in the presence of 50 μM lauric acid. Fig. 21, Fig. 25 (both expressed as turnover number).

Maximal transport rate (V_{max} – Lineweaver-Burk) for proton transport was 42.1 μmol $H^+min^{-1}mg^{-1}$ i.e. **40.3%** of the wt.. Value of Michaelis-Menten constant (K_m - Lineweaver-Burk) was 107.2 μM. Fig. 20, Fig. 23, Fig. 24.

Data from linear regression of H^+ transport as a function of UCP1 concentration, at different concentrations of lauric acid: Maximal transport rate (V_{max} – Lineweaver-Burk) for proton transport was 13.5 μmol $H^+min^{-1}mg^{-1}$ i. e. **72.9%** of the wt. Value of Michaelis-Menten constant (K_m - Lineweaver-Burk) was 184.8 μM. Fig. 22, Fig. 26.

The values of proton transport at extrapolation of lauric acid concentration to 100 μM: 4.613 μmol $H^{+}min^{-1}mg^{-1}$ (**34.3%** of wt). Fig. 26.

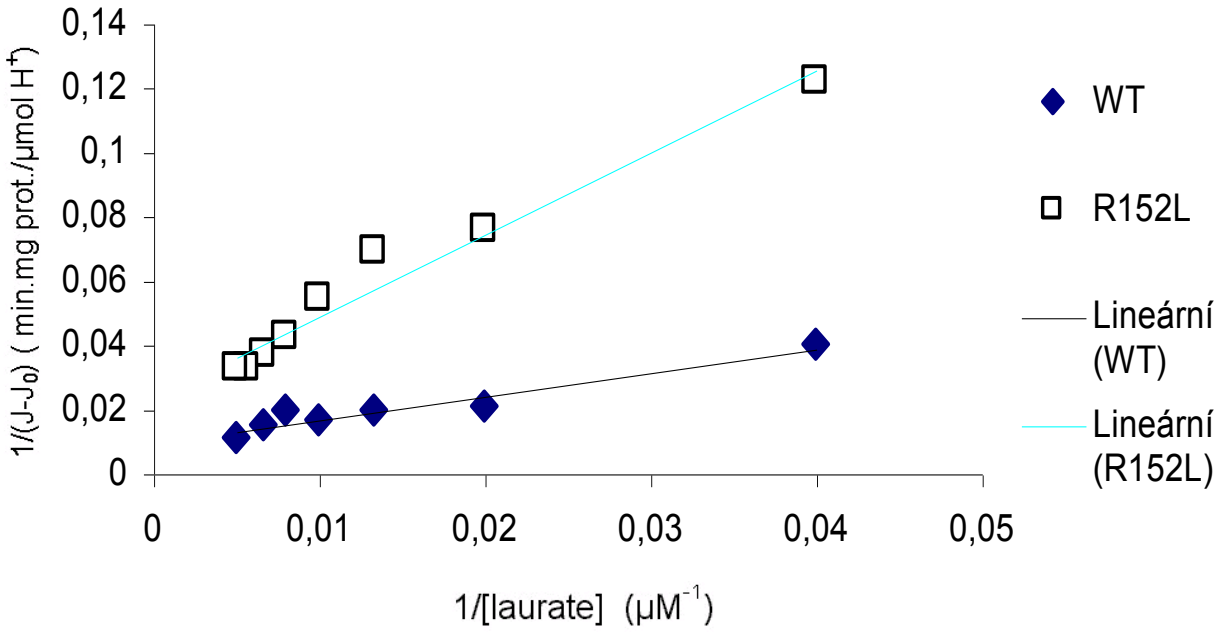

Fig. 20: The comparison of lauric acid activated - proton efflux kinetics of UCP1 wt and UCP1 R152L mutant is shown as double reciprocal (Lineweaver – Burk) plot. The flux J_0, caused by valinomycin in the absence of lauric acid, was subtracted

.

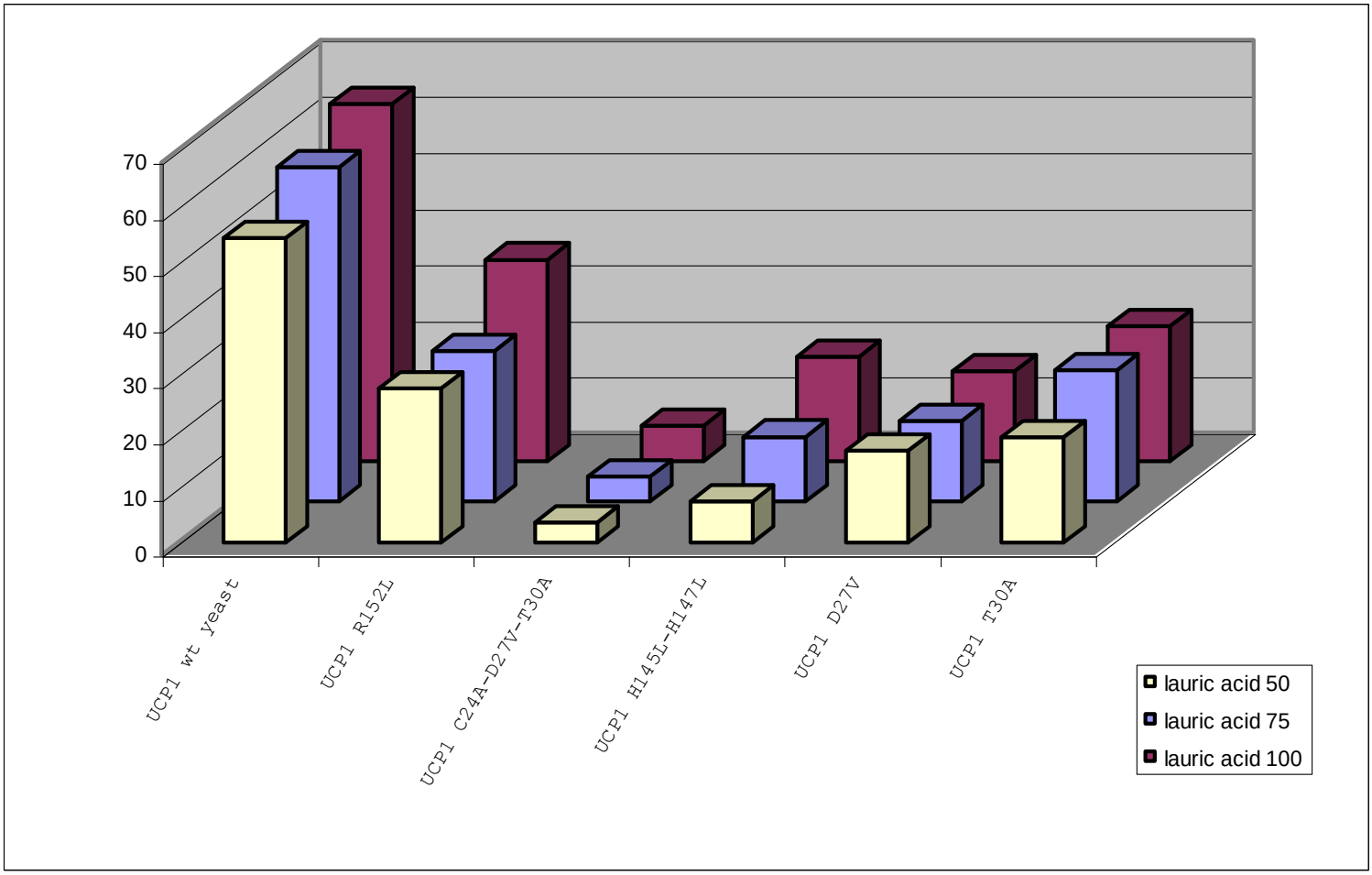

Fig.21: Comparison of H^+ transport turnover number [s^{-1}] of wild type and mutated UCP1 species at 50, 75 and 100 μM concentration of lauric acid.

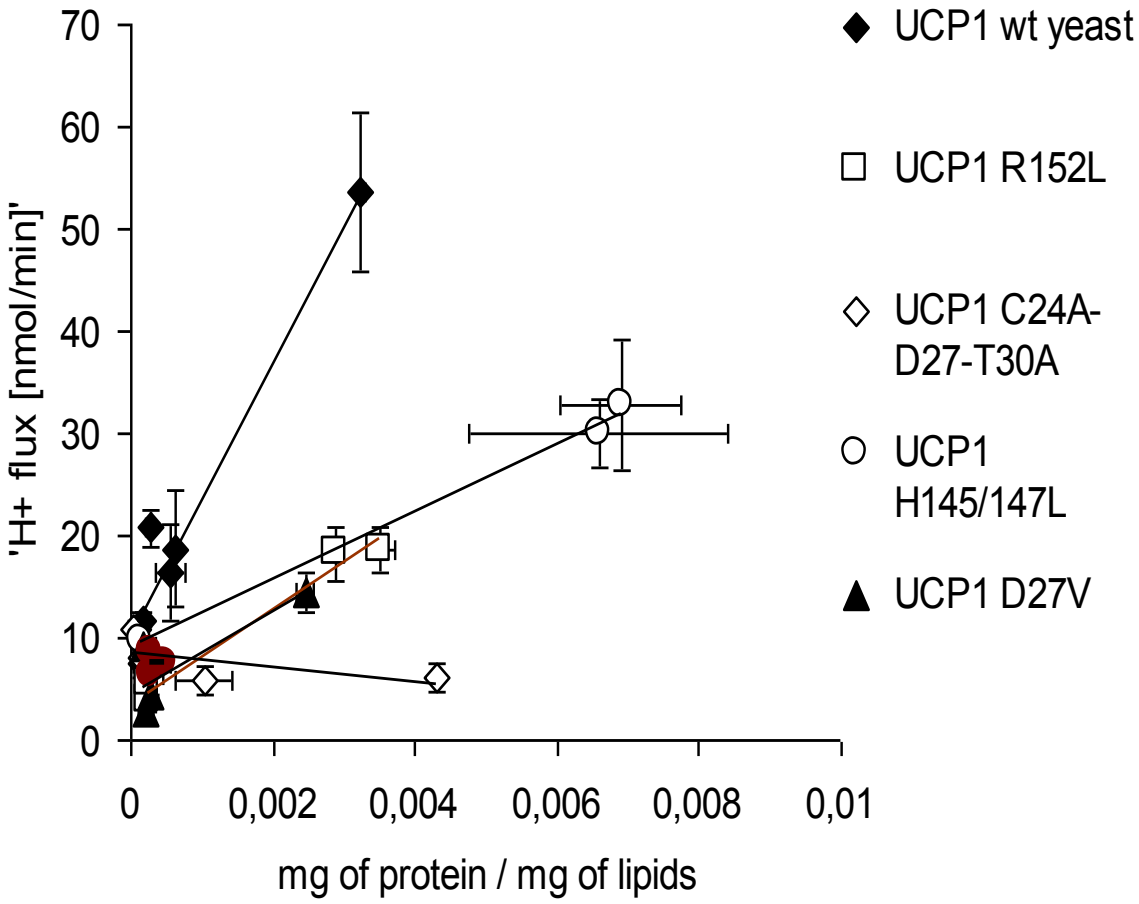

Fig. 22: H^+ transport as a function of UCP1 (wt or mutated species) amount relative to the amount of phospholipids in the proteoliposome. Parallels (corresponding to increasing concentration of lauric acid) of the slope of the H^+ transport response to the UCP1 amount were used for computation of "smoothed" kinetic or transport characteristics of wt and mutated UCP1 species. Negative trend of this function in case of C24AD27VT30A UCP1 is the reason of negative final values of these parameters for C24AD27VT30A mutant.

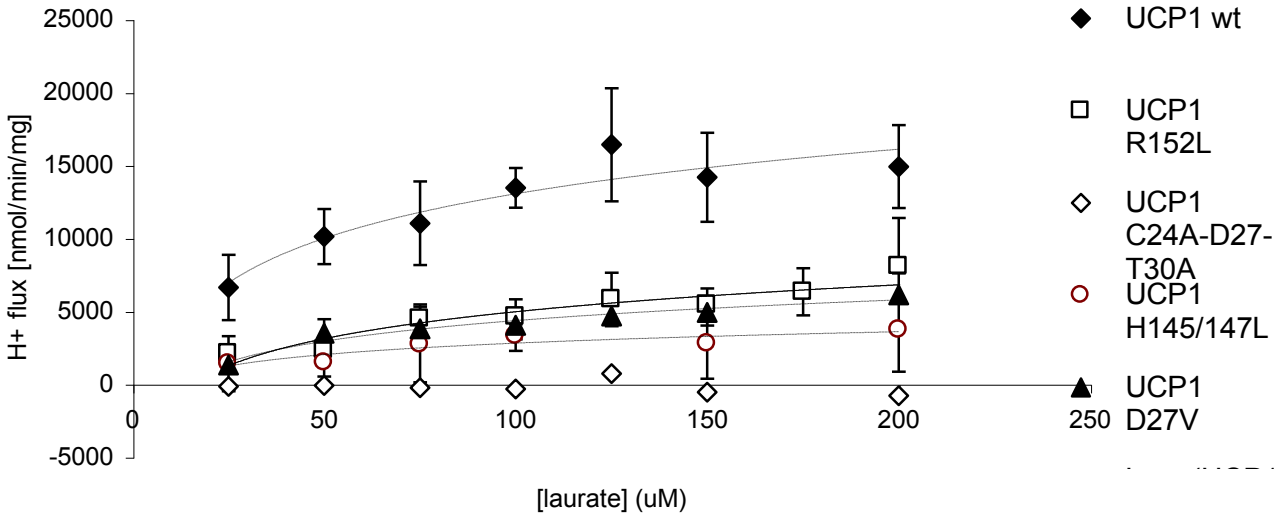

Fig. 23: Michaelis – Menten plot of H^+ transport of wild type and mutated UCP1 species as a function of concentration of lauric acid. Data generated by linear regression of H^+ transport as a function of UCP1 concentration were used as Y-values

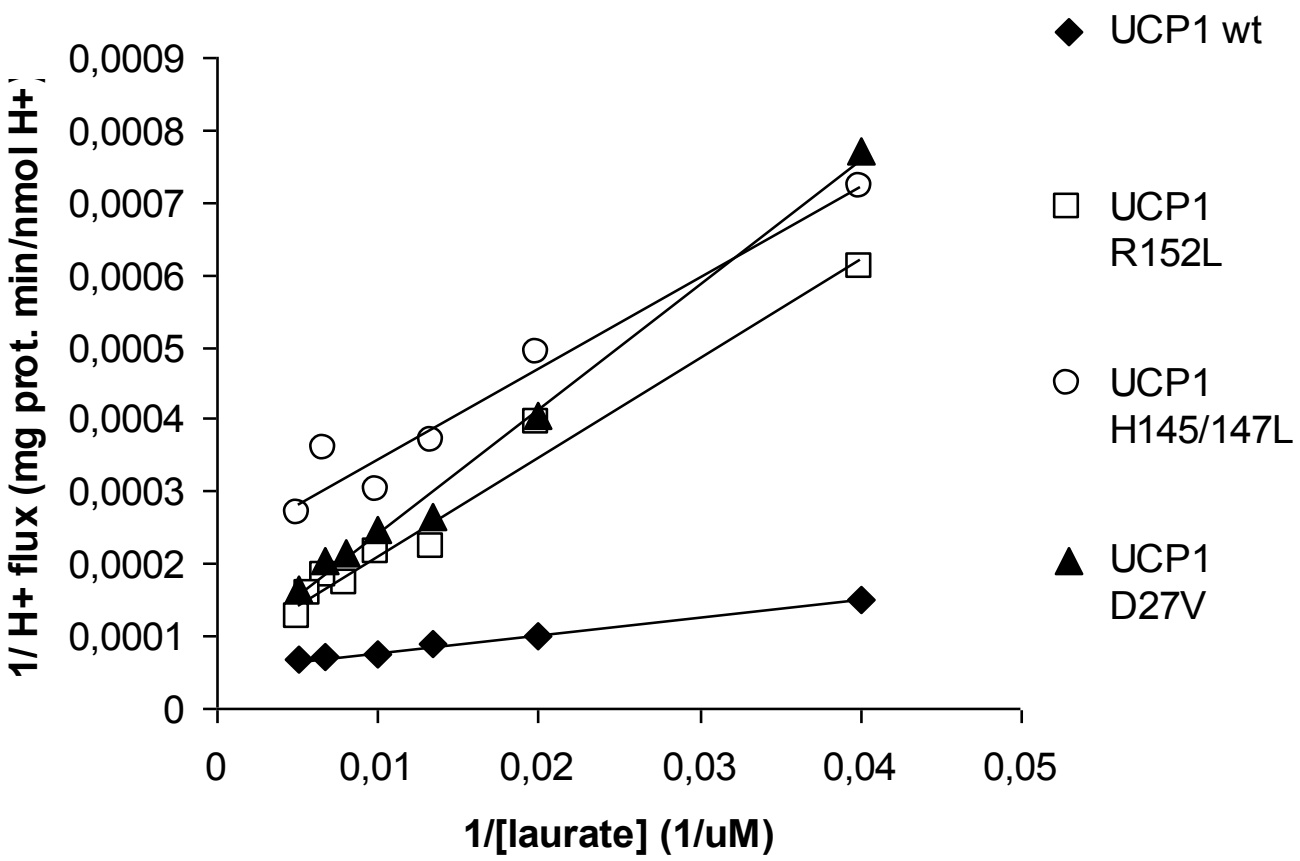

Fig. 24: Comparison of H^+ transport of wt and mutated UCP1 species as a function of lauric acid concentration; shown as double reciprocal (Lineweaver – Burk) plot. Data generated by linear regression of H^+ transport as a function of UCP1 concentration were used as Y-values

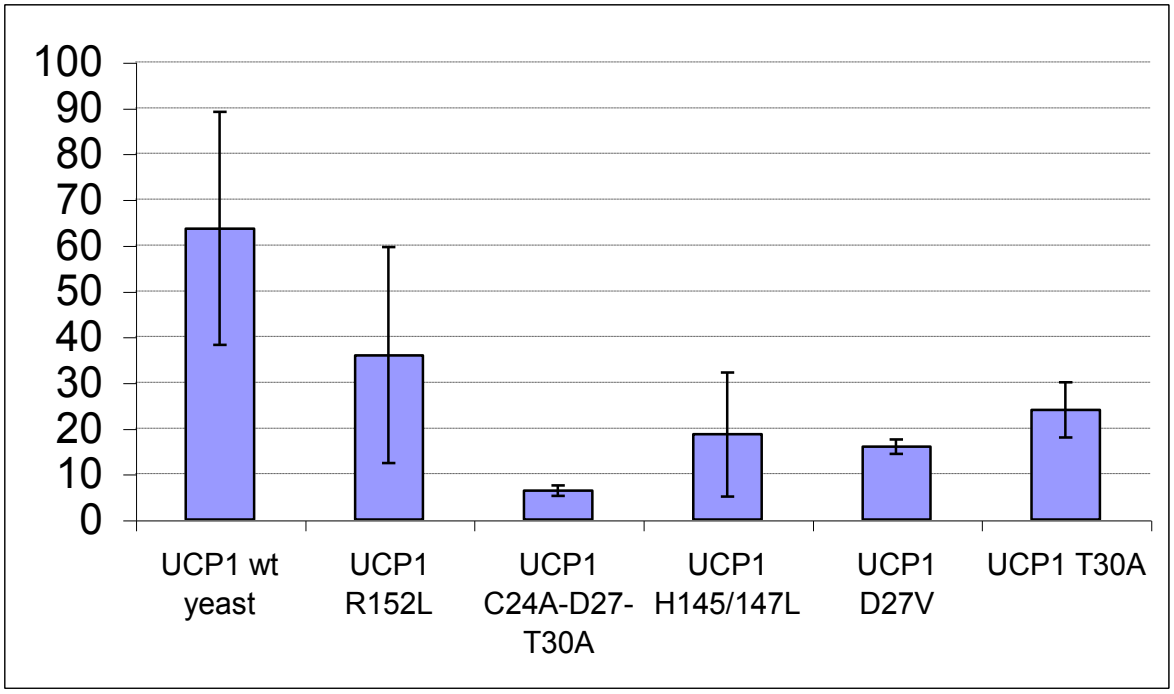

Fig. 25: Comparison of H^+ transport turnover number [s^{-1}] of wild type and mutated UCP1 species at 100 μM concentration of lauric acid.

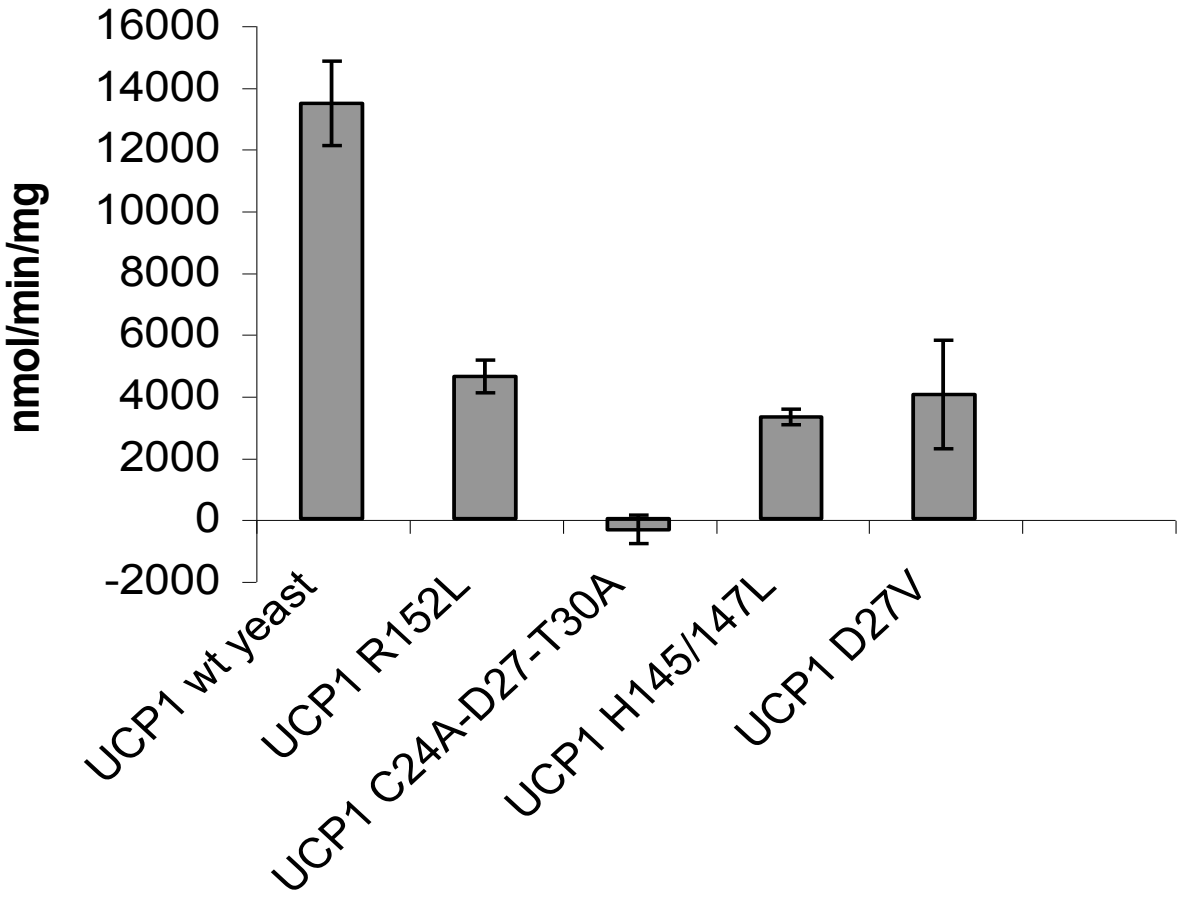

Fig. 26: Rates of lauric acid induced H+ uniport for various UCP1 mutants. Rates of uniport induced by 100 μM lauric acid per mg of protein were taken as slopes of the protein dependence shown in Fig. 22, calculated using linear regression.

4.2.7 Cl^- transport characteristics

For characteristics of Cl^- transport see article [110] in Appendix.

4.2.8 NTP binding

For characteristic of ^{3}H-GTP binding see article [110] in Appendix

5 Discussion

5.1 Involvement of mutated AA residues in proton transport and regulation

Sections of highly conserved sequence (so called signatures) are of high importance also during the process of selecting positions for mutational AA substitutions. Interpretation of impairment of function caused by such substitution is more straightforward, as there is relatively high probability that the residue within the signature plays direct role in the function. Thus, the effect of exchange is probably not due to change of conformation of the whole molecule.

One of conserved and unique AA residues is Arg 152. In this study for the first time elimination of its positive charge at this position is assessed. This exchange resulted in roughly 50% reduction of V_{max} for FA-induced H^+ uniport and of apparent affinity for lauric acid. Elimination of close charge Lys 150 did not lead to similar changes (Urbánková et al., unpublished results). Cl^- translocation as well as binding of ^{3}H-GTP were uninfluenced. Interpretation of this finding can be or direct or in terms of conformational change, possibly also as sterical hindrance. As this residue encompasses into unique conserved sequence, direct involvement in proton transport function is preferred explanation.

The second studied region is also located on the second matrix segment, but outside the UCP signature. For UCP1 it contains a His pair H145 and H147. Here is confirmed the result of group of Klingenberg [91] that the substitution of both His in our H145 and H147 mutant lead to the fatty acid induced uniport with V_{max} reduced by 70% and affinity to fatty acids reduced to 50% values. The Cl^- uniport and ^{3}H-GTP binding remained uninfluenced. Previously, this was interpreted in terms of direct His participation in the presumed H^+ translocation via UCP1 [91]. But the studied His pair exists only in UCP1, whereas UCP3 has only one His, and other UCPs contain no His in this location [23,111]. Consequently, the interpretation in terms of (local) conformational changes or sterical hindrances is more acceptable in this case. The conformational changes could even affect distant AA residues of the second matrix UCP-signature such as the above discussed Arg152.

The second studied area was the UCP-signature in the first α-helix. Two important polar residues Asp27 and Thr30as well as all its polar AARs altogether (in the triple C24A and D27V and T30A mutant) were substituted. It is noteworthy that the substitution of Cys24 did not lead to phenotype

changes [90]. The previous D27N substitution (i.e. neutralization of the only negative change in this UCP-signature) resulted in a nearly complete elimination of the FA-induced H^+ uniport while the Cl^- uniport was preserved [87]. Although this was later questioned [112], the importance of Asp27 has been confirmed by obtaining ~50% reduction of V_{max} for H^+ uniport and by demonstrating the four times lowered FA affinity for prepared D27V mutant.

The role of T30 within this area still remains enigmatic as the results obtained from first measurements at different concentrations of fatty acids display the response of the transport rate to concentration of fatty acids as well as more than 50% decrease of proton transport. On the contrary, results later published by Urbánková et al. [110] claim no influence of the T30A substitution on proton transport. In agreement there is a decrease of the affinity to fatty acids (3.5 times, 2.5 times respectively).

The substitution of all three polar AA residues of the first α-helix UCP-signature has not completely eliminated the fatty acid induced H^+ uniport, whereas K_d for ^{3}H-GTP binding remained constant. The most probable interpretation for Asp27 could be conformational change subsequently affecting the final type. Asp27 may stabilize UCP-conformation by means of ion interaction with some positively charged AA residues of any neighbor α-helix or matrix segment.

5.2 Mechanism of uncoupling

New view on the mechanism of shunting the electrochemical potential by UCP1 was brought by Klingenberg as integration of roles of FAs and newly discovered and confirmed necessity of interaction of CoQ for proton transport. Controversy remains whether fatty acids transport protons by flip-flop mechanism as described in the introduction of this dissertation or if they just provide COO^- to fill supposed carboxyl-deficient gap within the proton transport pathway formed as a result of particular UCP1 conformation (FA-buffering hypothesis). There are findings supporting fatty acid cycling (flip-flop) as well as findings strongly supporting the FA-buffering hypothesis. Substantial difference between transport rates of H^+ and non-physiological transport of halide anions is often mentioned as an argument against versatile mechanism of translocation (i.e. FA cycling [flip-flop] mechanism). Another argument indirectly supporting FA-buffering hypothesis is promotion of H^+ transport by derivatives of fatty acids conjugated to bulky moieties, thus unable to freely pass through the inner mitochondrial membrane. The pH dependency of FA

activation of proton transport as well as quite critical role of protonable residues in this process should also serve as a strong proof in favour of FA-buffering [84] .

Now, new, modified model was postulated. In this model fatty acid interacts by its headgroups with CoQ headgroup and originally undissociated carboxyl group of fatty acid forms hydrogen bond with the oxo-group of CoQ. This reaction is accompanied by release of H^+, which is in such a way "inserted" into proton transport pathway of UCP1 [113].

Patch-clamp experiments done one variety of MACPs, including UCP1 uncovered phenomenon of channel behavior of these proteins under certain conditions. Then two issues need to be solved: 1st How can FA cycling ensure transport velocities of such level, and 2nd How can be transport via hydrophilic pathway (FA-buffering hypothesis) under carrier–like parameters converted into transport with properties of channel.

First alternative (FA cycling) is dismissed as complete side-effect, as there are FA^- translocated in the MACP-phospholipid interface not only by UCP, but also by other MACPs with clearly defined transport function.

Concerning second possibility of transformation of hydrophilic proton transport pathway into channel, model of two gates (one on each side), controlling permeability of this pathway, is suggested. The α-helices of UCP1 should form walls of hydrophilic pathway, while short α-helix at the N-terminus comprising residues 262 – 268 should be critical for control of carrier/channel mode. This short α-helix is in position perpendicular to the 6th transmembrane α-helix and mutations in hinge region connecting these two helices turned out to cause transition from carrier into channel [84].

5.3 Evolutionary aspects

Results of this work can help in better understanding of two basic aspects of proteins from UCP subfamily: their function and their emergence in evolution. Conclusions concerning first appearance of UCP proteins can be made only in indirect way based on the fact that first members of MACP family did not emerged earlier than in eucaryotes [17] and on findings of UCPs in early, relatively primitive multicellular eucaryotes [21,22,111]. This dates first appearance of UCPs on evolutionary scale. Search through DNA sequences of unicellular eucaryotes would be needed to give more detailed answer about their origin. Ongoing sequencing projects especially of some unicellular eucaryotic parasites could soon provide material for such effort.

When one of the five up to now known members of the UCP family is postulated as ancestral one because of widespread occurrence of its modifications (orthologs) throughout multicellular organisms, or when at least different genuinity of each of UCP family members is hypothesised, new question of how the putativelly derived UCP member like UCP1 coevolved together with the mechanism of highly specialized thermogenesis (including specialized tissue, regulation via sympathetic nervous system, involvement of locally produced NE etc.) is raised. As the BAT is referred only in mammals, this question seems to be of bigger complexness than similar questions concerning much more complicated organs, which are however widespread throughout all vertebrates. Basic similarity might be seen with the mechanism of specific immunity, reaching its top in mammals and birds – homoiothermic organisms. The immune system also represents sophisticated physiological mechanism comprising number of precisely tuned feedback relations. Moreover, there is growing knowledge about mutual interconnections among mechanisms of thermogenesis, body weight control and immunity. To get more solid ground for these speculations, spectrum of UCP sequences, including their exon/intron architecture, as well as sequences of their promotors and enhancers, from birds and also reptiles (some of extinct reptile species are believed to be homoiothermic) would be necessary.

In some communications the occurrence of BMCP1/UCP5L in testis is speculated to be forced be need of highly regulated temperature as temperature is one of critical factors in the process of spermatogenesis. When this speculation is put into the context of another facts, the explanation needs to be more complex. From the evolutional point of view the scrotum was formed and testis moved into it just to provide for the spermatogenesis lower temperature than is the temperature of the whole body. Hence, the putative thermogenic function of BMCP1/UCP5L in testis seems to be contradictory to need of lower temperature. However, separation from the mass of the whole body does not mean only decrease of temperature but also the higher variation as the "buffering" capacity of the whole body cannot be exploited. Extra mechanism of thermogenesis can be necessary in such case. BMCP1/UCP5L could play the role of such mechanism. This mechanism, if confirmed, resembles in certain aspects role suggested for UCP3 in muscles i.e. buffering declines of heat production of BAT [35].

6 Conclusions

- Matching previously known UCP sequences to genome and protein databases uncovered new UCP homologs. Four UCP sequences were found in fly *Drosophila melanogaster*, one in nematode *Caenorhabditis elegans*, one in *Dictyostelium discoideum* and one new UCP in plant *Arabidopsis thaliana* [111].
- Three UCP1 mutants from the 1st α–helix (D27V, T30A and C24A-D27V-T30A) and two from the second matrix segment (H145L-H147L and R152L) were constructed, expressed and incorporated into proteoliposomes with entrapped H^+ and Cl^- indicator.
- By the same procedure proteoliposomes with wild type UCP1 were prepared. The transport properties of wt UCP1 were in agreement with the values published [59,109,114].
- All constructed mutant UCP1 species displayed neither any changes (when compared to the wild type) in their Cl^- transport characteristics, nor their nucleotide binding affinity was changed.
- In mutants D27V, T30A* and R152L V_{max} value for H^+ transport was reduced at least to 50%
- In mutant C24A-D27V-T30A H^+ transport was impaired in absolute way.
- The affinity for lauric acid (K_m) was reduced in all mutants; in H145L-H147L, based just on the data from the dissertation, the reduction of K_m is in doubt.

* Proton transport data of this mutant presented in this dissertation do not correspond to values presented in article 110. Author of this dissertation can guarantee just the data presented here, irrespectively of the fact, that data in the article are based on much more extensive set of measurements so that should characterize the mutant in more objective way. Further measurements would be beneficial to confirm H^+ transport characteristics of T30A UCP1.

7 Acknowledgements

Mgr. Eva Urbánková is the person who shared my intention of finishing the process of preparation of UCP1 mutants by producing set of data characterizing each of them. She taught me methods of preparation of proteoliposomes and measurement of transport. Collaboration with her was excellent.

I am also obliged to Dr. Čestmír Vlček, who operated ALF Pharmacia DNA sequencer, made staining of sequencing primers and was exceptionally helpful in explaining any topic concerning this part of DNA techniques.

I should express my gratitude to Dr. Eva Škobisová, who was doing the binding studies, as well as to all the people in the lab for sharing the laboratory space with me.

I would like to thank my wife Martina especially for her substantial help on the final layout of the essay as well as for her critical comments concerning unfit pieces of the text. Also I thank to my family. I devote this dissertation to the memory of my mother Markéta Hanáková.

8 Abbreviations

AA	amino acids(s)
AAC	ADP/ATP Carrier
AAr	amino acid residue
ATP	adenosinetriphosphate
BLAST	Basic Local Alignment Search Tool
BMCP	Brain Mitochondrial Carrier Protein
BRE	Brown Fat Regulatory Element
bp	base pair
BSA	bovine serum albumin
cAMP	cyclic adenosinemonophosphate
CRE	cAMP Response Element
CCCP	carbonylcyanide-3-chlorophenylhydrazone
FCCP	carbonylcyanide-4-trifluoro-methoxyphenylhydrazone
GDP	guanosinediphosphate
GTP	guanosinetriphosphate
C/EBP	CCAAT/Enhancer Binding Protein
CoQ	coenzyme Q
CRE	cAMP Response Element
CREB	CRE Binding Protein
DANSYL	5-dimethylaminoaphthalene-1-sulfonyl
EDTA	ethylenediaminetetraacetic acid
EGTA	ethylene glycol bis (2-amino-ethylenether)N,N,N',N'-tetra acetic acid
ELPHO	electrophoresis
EtBr	ethidium bromide
FA	fatty acid
FCCP	carbonylcyanide-4-trifluoro-methoxyphenylhydrazone
HEPES	4-(2-hydroxyethyl)piperazine-1-ethanesulfonic acid
IGF	Insulin like Growth Factor
MACP	Mitochondrial Anion Carrier Protein
NDP	nucleotide diphosphate

NTP	nucleotide triphosphate
PAGE	PolyacrylAmide Gel Electrophoresis
PCR	Polymerase Chain Reaction
PMSF	phenylmethylsulfonyl fluoride
PN	purine nucleotide
PPARγ	peroxisome proliferation activating receptor γ
PUMP	plant uncoupling mitochondrial protein
RARE	retinoic acid response element
SDS	sodium dodecyl sulfate
SPQ	6-methoxy-N-(3-sulfopropyl)quinolinium
T_3	3,3',5-triiodo-L-thyronine
TEA	tetraethylammonium hydroxide
TES	N-tris(hydroxymethyl)methyl-2-aminoethanesulfonic acid
THRS	Thyroide Hormone Response Sequence
Tris	2-amino-2-hydroxymethyl-1,3-propanediol
UCP	Uncoupling Protein
URE1	UCP Regulatory Element 1
UV	Ultra Violet
WAT	white adipose tissue
WB	Western Blot
wt	wild type

9 Code for amino acids

A	Ala	**a**lanine
C	Cys	**c**ysteine
D	Asp	aspartic acid
E	Glu	glutamic acid
F	Phe	**ph**enylalanine
G	Gly	**g**lycine
H	His	**h**istidine
I	Ile	**i**soleucine
K	Lys	lysine
L	Leu	**l**eucine
M	Met	**m**ethionine
N	Asn	asparagi**n**e
P	Pro	**p**roline
Q	Gln	glutamine
R	Arg	a**r**ginine
S	Ser	**s**erine
T	Thr	**t**hreonine

10 References

1. Ricquier, D. & Bouillaud, F. The uncoupling protein homologues: UCP1, UCP2, UCP3, StUCP and AtUCP. *Biochem J* **345 Pt 2**, 161-79. (2000).
2. Kozak, U. C. & Kozak, L. P. Norepinephrine-dependent selection of brown adipocyte cell lines. *Endocrinology* **134**, 906-13. (1994).
3. Palou, A., Pico, C., Bonet, M. L. & Oliver, P. The uncoupling protein, thermogenin. *Int J Biochem Cell Biol* **30**, 7-11. (1998).
4. Nicholls, D. G. & Rial, E. A history of the first uncoupling protein, UCP1. *J Bioenerg Biomembr* **31**, 399-406. (1999).
5. Bianco, A. C., Sheng, X. Y. & Silva, J. E. Triiodothyronine amplifies norepinephrine stimulation of uncoupling protein gene transcription by a mechanism not requiring protein synthesis. *J Biol Chem* **263**, 18168-75. (1988).
6. Leonard, J. L., Mellen, S. A. & Larsen, P. R. Thyroxine 5'-deiodinase activity in brown adipose tissue. *Endocrinology* **112**, 1153-5. (1983).
7. Guerra, C., Benito, M. & Fernandez, M. IGF-I induces the uncoupling protein gene expression in fetal rat brown adipocyte primary cultures: role of C/EBP transcription factors. *Biochem Biophys Res Commun* **201**, 813-9. (1994).
8. Yubero, P. et al. CCAAT/enhancer binding proteins alpha and beta are transcriptional activators of the brown fat uncoupling protein gene promoter. *Biochem Biophys Res Commun* **198**, 653-9. (1994).
9. Nedergaard, J. & Cannon, B. in *New Comprehensive Biochemistry, Molecular Mechanisms in Bioenergetics* (ed. L., E.) 385 - 420 (Elsevier, Amsterdam, 1992).
10. Ricquier, D. et al. Expression of uncoupling protein mRNA in thermogenic or weakly thermogenic brown adipose tissue. Evidence for a rapid beta- adrenoreceptor-mediated and transcriptionally regulated step during activation of thermogenesis. *J Biol Chem* **261**, 13905-10. (1986).
11. Enerback, S. et al. Mice lacking mitochondrial uncoupling protein are cold-sensitive but not obese. *Nature* **387**, 90-4. (1997).
12. Kopecky, J., Clarke, G., Enerback, S., Spiegelman, B. & Kozak, L. P. Expression of the mitochondrial uncoupling protein gene from the aP2 gene promoter prevents genetic obesity. *J Clin Invest* **96**, 2914-23. (1995).

13. Skulachev, V. P. Uncoupling: new approaches to an old problem of bioenergetics. *Biochim Biophys Acta* **1363**, 100-24. (1998).
14. Rafael, J. & Heldt, H. W. Binding of guanine nucleotides to the outer surface of the inner membrane of guinea pig brown fat mitochondria in correlation with the thermogenic activity of the tissue. *FEBS Lett* **63**, 304-8. (1976).
15. Nicholls, D. G. Hamster brown-adipose-tissue mitochondria. Purine nucleotide control of the ion conductance of the inner membrane, the nature of the nucleotide binding site. *European Journal of Biochemistry* **62**, 223-8 (1976).
16. Klingenberg, O. in *Chemistry, Biochemistry and Toxicology* 69-107 (Picin Medical Books, Padova, 1978).
17. Klingenberg, M. Mechanism and evolution of the uncoupling protein of brown adipose tissue. *Trends Biochem Sci* **15**, 108-12. (1990).
18. Aquila, H., Link, T. A. & Klingenberg, M. Solute carriers involved in energy transfer of mitochondria form a homologous protein family. *FEBS Lett* **212**, 1-9. (1987).
19. Klaus, S., Casteilla, L., Bouillaud, F. & Ricquier, D. The uncoupling protein UCP: a membraneous mitochondrial ion carrier exclusively expressed in brown adipose tissue. *Int J Biochem* **23**, 791-801 (1991).
20. Pecqueur, C. et al. Functional organization of the human uncoupling protein-2 gene, and juxtaposition to the uncoupling protein-3 gene. *Biochem Biophys Res Commun* **255**, 40-6. (1999).
21. Jarmuszkiewicz, W., Sluse-Goffart, C. M., Hryniewiecka, L. & Sluse, F. E. Identification and characterization of a protozoan uncoupling protein in Acanthamoeba castellanii. *J Biol Chem* **274**, 23198-202. (1999).
22. Jarmuszkiewicz, W. et al. First evidence and characterization of an uncoupling protein in fungi kingdom: CpUCP of Candida parapsilosis. *FEBS Lett* **467**, 145-9. (2000).
23. Jezek, P. & Urbankova, E. Specific sequence of motifs of mitochondrial uncoupling proteins. *IUBMB Life* **49**, 63-70. (2000).
24. Boss, O. et al. Tissue-dependent upregulation of rat uncoupling protein-2 expression in response to fasting or cold. *FEBS Lett* **412**, 111-4. (1997).
25. Zhou, Y. T. et al. Induction by leptin of uncoupling protein-2 and enzymes of fatty acid oxidation. *Proc Natl Acad Sci U S A* **94**, 6386-90. (1997).
26. Gimeno, R. E. et al. Cloning and characterization of an uncoupling protein homolog: a potential molecular mediator of human thermogenesis. *Diabetes* **46**, 900-6. (1997).

27. Fleury, C. et al. Uncoupling protein-2: a novel gene linked to obesity and hyperinsulinemia. *Nat Genet* **15**, 269-72. (1997).
28. Boss, O. et al. Uncoupling protein-3: a new member of the mitochondrial carrier family with tissue-specific expression. *FEBS Lett* **408**, 39-42. (1997).
29. Jaburek, M. et al. Transport function and regulation of mitochondrial uncoupling proteins 2 and 3. *J Biol Chem* **274**, 26003-7. (1999).
30. Larrouy, D. et al. Kupffer cells are a dominant site of uncoupling protein 2 expression in rat liver. *Biochem Biophys Res Commun* **235**, 760-4. (1997).
31. Hodny, Z. et al. High expression of uncoupling protein 2 in foetal liver. *FEBS Lett* **425**, 185-90. (1998).
32. Gong, D. W., He, Y., Karas, M. & Reitman, M. Uncoupling protein-3 is a mediator of thermogenesis regulated by thyroid hormone, beta3-adrenergic agonists, and leptin. *J Biol Chem* **272**, 24129-32. (1997).
33. Weigle, D. S. et al. Elevated free fatty acids induce uncoupling protein 3 expression in muscle: a potential explanation for the effect of fasting. *Diabetes* **47**, 298-302. (1998).
34. Clapham, J. C. et al. Mice overexpressing human uncoupling protein-3 in skeletal muscle are hyperphagic and lean. *Nature* **406**, 415-8. (2000).
35. Boss, O. et al. Uncoupling protein-3 expression in rodent skeletal muscle is modulated by food intake but not by changes in environmental temperature. *J Biol Chem* **273**, 5-8. (1998).
36. Hinz, W., Gruninger, S., De Pover, A. & Chiesi, M. Properties of the human long and short isoforms of the uncoupling protein-3 expressed in yeast cells. *FEBS Lett* **462**, 411-5. (1999).
37. Zhang, C. Y., Hagen, T., Mootha, V. K., Slieker, L. J. & Lowell, B. B. Assessment of uncoupling activity of uncoupling protein 3 using a yeast heterologous expression system. *FEBS Lett* **449**, 129-34. (1999).
38. Laloi, M. et al. A plant cold-induced uncoupling protein. *Nature* **389**, 135-6. (1997).
39. Maia, I. G. et al. AtPUMP: an Arabidopsis gene encoding a plant uncoupling mitochondrial protein. *FEBS Lett* **429**, 403-6. (1998).
40. Watanabe, A., Nakazono, M., Tsutsumi, N. & Hirai, A. AtUCP2: a novel isoform of the mitochondrial uncoupling protein of Arabidopsis thaliana. *Plant Cell Physiol* **40**, 1160-6. (1999).

41. Ito, K. Isolation of two distinct cold-inducible cDNAs encoding plant uncoupling proteins from spadix of skunk cabbage (Symplocarpus foetidus). *Plant Science* **149**, 167 - 173 (1999).
42. Jezek, P. et al. Fatty acid cycling mechanism and mitochondrial uncoupling proteins. *Biochim Biophys Acta* **1365**, 319-27. (1998).
43. Jezek, P., Costa, A. D. & Vercesi, A. E. Evidence for anion-translocating plant uncoupling mitochondrial protein in potato mitochondria. *J Biol Chem* **271**, 32743-8. (1996).
44. Jezek, P., Costa, A. D. & Vercesi, A. E. Reconstituted plant uncoupling mitochondrial protein allows for proton translocation via fatty acid cycling mechanism. *J Biol Chem* **272**, 24272-8. (1997).
45. Sanchis, D. et al. BMCP1, a novel mitochondrial carrier with high expression in the central nervous system of humans and rodents, and respiration uncoupling activity in recombinant yeast. *J Biol Chem* **273**, 34611-5. (1998).
46. Yu, X. X. et al. Characterization of novel UCP5/BMCP1 isoforms and differential regulation of UCP4 and UCP5 expression through dietary or temperature manipulation. *Faseb J* **14**, 1611-8. (2000).
47. Mao, W. et al. UCP4, a novel brain-specific mitochondrial protein that reduces membrane potential in mammalian cells. *FEBS Lett* **443**, 326-30. (1999).
48. Jezek, P. & Garlid, K. D. Mammalian mitochondrial uncoupling proteins. *Int J Biochem Cell Biol* **30**, 1163-8. (1998).
49. Lin, C. S. & Klingenberg, M. Characteristics of the isolated purine nucleotide binding protein from brown fat mitochondria. *Biochemistry* **21**, 2950-6. (1982).
50. Ricquier, D. & Kader, J. C. Mitochondrial protein alteration in active brown fat: a soidum dodecyl sulfate-polyacrylamide gel electrophoretic study. *Biochem Biophys Res Commun* **73**, 577-83. (1976).
51. Rial, E., Muga, A., Valpuesta, J. M., Arrondo, J. L. & Goni, F. M. Infrared spectroscopic studies of detergent-solubilized uncoupling protein from brown-adipose-tissue mitochondria. *Eur J Biochem* **188**, 83-9. (1990).
52. Lin, C. S., Hackenberg, H. & Klingenberg, E. M. The uncoupling protein from brown adipose tissue mitochondria is a dimer. A hydrodynamic study. *FEBS Lett* **113**, 304-6. (1980).

53. Jacobsson, A., Stadler, U., Glotzer, M. A. & Kozak, L. P. Mitochondrial uncoupling protein from mouse brown fat. Molecular cloning, genetic mapping, and mRNA expression. *J Biol Chem* **260**, 16250-4. (1985).
54. Otsen, M., Den Bieman, M. & van Zutphen, L. F. Linkage of the gene for uncoupling protein to esterase-1,2 and haptoglobin in the rat. *J Hered* **84**, 149-51. (1993).
55. Cassard, A. M. et al. Human uncoupling protein gene: structure, comparison with rat gene, and assignment to the long arm of chromosome 4. *J Cell Biochem* **43**, 255-64. (1990).
56. Bouillaud, F., Raimbault, S. & Ricquier, D. The gene for rat uncoupling protein: complete sequence, structure of primary transcript and evolutionary relationship between exons. *Biochem Biophys Res Commun* **157**, 783-92. (1988).
57. Heaton, G. M., Wagenvoord, R. J., Kemp, A., Jr. & Nicholls, D. G. Brown-adipose-tissue mitochondria: photoaffinity labelling of the regulatory site of energy dissipation. *Eur J Biochem* **82**, 515-21. (1978).
58. Gonzalez-Barroso, M. M. et al. Structural and functional study of a conserved region in the uncoupling protein UCP1: the three matrix loops are involved in the control of transport. *J Mol Biol* **292**, 137-49. (1999).
59. Jezek, P. & Garlid, K. D. New substrates and competitive inhibitors of the Cl- translocating pathway of the uncoupling protein of brown adipose tissue mitochondria. *J Biol Chem* **265**, 19303-11. (1990).
60. Nicholls, D. G. & Lindberg, O. Brown-adipose-tissue mitochondria. The influence of albumin and nucleotides on passive ion permeabilities. *Eur J Biochem* **37**, 523-30. (1973).
61. Jezek, P. & Borecky, J. Mitochondrial uncoupling protein may participate in futile cycling of pyruvate and other monocarboxylates. *Am J Physiol* **275**, C496-504. (1998).
62. Matthias, A., Jacobsson, A., Cannon, B. & Nedergaard, J. The bioenergetics of brown fat mitochondria from UCP1-ablated mice. Ucp1 is not involved in fatty acid-induced de-energization ("uncoupling"). *J Biol Chem* **274**, 28150-60. (1999).
63. Klingenberg, M. Nucleotide binding to uncoupling protein. Mechanism of control by protonation. *Biochemistry* **27**, 781-91. (1988).
64. French, R. R., Gore, M. G. & York, D. A. A study of GDP binding to purified thermogenin protein from brown adipose tissue. *Biochem J* **251**, 385-9. (1988).

65. Fernandez, M., Nicholls, D. G. & Rial, E. The uncoupling protein from brown-adipose-tissue mitochondria. Chymotrypsin-induced structural and functional modifications. *Eur J Biochem* **164**, 675-80. (1987).
66. Eckerskorn, C. & Klingenberg, M. In the uncoupling protein from brown adipose tissue the C-terminus protrudes to the c-side of the membrane as shown by tryptic cleavage. *FEBS Lett* **226**, 166-70. (1987).
67. Cannon, B., Nicholls, D.G., Lindberg, O. (ed. al., G. F. A. e.) 357 - 364 (Academic Press, New York, 1973).
68. Nicholls, D. G. The bioenergetics of brown adipose tissue mitochondria. *FEBS Letters* **61**, 103-110 (1976).
69. Nicholls, D. G. Hamster brown-adipose-tissue mitochondria. The chloride permeability of the inner membrane under respiring conditions, the influence of purine nucleotides. *Eur J Biochem* **49**, 585-93. (1974).
70. Nicholls, D. G., Bernson, V. S. & Heaton, G. M. The identification of the component in the inner membrane of brown adipose tissue mitochondria responsible for regulating energy dissipation. *Experientia Suppl* **32**, 89-93 (1978).
71. Murdza-Inglis, D. L. et al. Functional reconstitution of rat uncoupling protein following its high level expression in yeast. *J Biol Chem* **266**, 11871-5. (1991).
72. Jezek, P., Houstek, J. & Drahota, Z. Alkaline pH, membrane potential, and magnesium cations are negative modulators of purine nucleotide inhibition of H+ and Cl- transport through the uncoupling protein of brown adipose tissue mitochondria. *J Bioenerg Biomembr* **20**, 603-22. (1988).
73. Kopecky, J., Jezek, P., Drahota, Z. & Houstek, J. Control of uncoupling protein in brown-fat mitochondria by purine nucleotides. Chemical modification by diazobenzenesulfonate. *Eur J Biochem* **164**, 687-94. (1987).
74. Kopecky, J., Guerrieri, F., Jezek, P., Drahota, Z. & Houstek, J. Molecular mechanism of uncoupling in brown adipose tissue mitochondria. The non-identity of proton and chloride conducting pathways. *FEBS Lett* **170**, 186-90. (1984).
75. Rial, E., Arechaga, I., Sainz-de-la-Maza, E. & Nicholls, D. G. Effect of hydrophobic sulphydryl reagents on the uncoupling protein and inner-membrane anion channel of brown-adipose-tissue mitochondria. *Eur J Biochem* **182**, 187-93. (1989).
76. Rial, E., Poustie, A. & Nicholls, D. G. Brown-adipose-tissue mitochondria: the regulation of the 32000-Mr uncoupling protein by fatty acids and purine nucleotides. *Eur J Biochem* **137**, 197-203. (1983).

77. Klingenberg, M. & Huang, S. G. Structure and function of the uncoupling protein from brown adipose tissue. *Biochim Biophys Acta* **1415**, 271-96. (1999).
78. Skulachev, V. P. Chemiosmotic systems in bioenergetics: H(+)-cycles and Na(+)-cycles. *Biosci Rep* **11**, 387-441; discussion 441-4. (1991).
79. Garlid, K. D., Orosz, D. E., Modriansky, M., Vassanelli, S. & Jezek, P. On the mechanism of fatty acid-induced proton transport by mitochondrial uncoupling protein. *J Biol Chem* **271**, 2615-20. (1996).
80. Jezek, P., Modriansky, M. & Garlid, K. D. Inactive fatty acids are unable to flip-flop across the lipid bilayer. *FEBS Lett* **408**, 161-5. (1997).
81. Jezek, P., Modriansky, M. & Garlid, K. D. A structure-activity study of fatty acid interaction with mitochondrial uncoupling protein. *FEBS Lett* **408**, 166-70. (1997).
82. Murdza-Inglis, D. L. et al. A single mutation in uncoupling protein of rat brown adipose tissue mitochondria abolishes GDP sensitivity of H+ transport. *J Biol Chem* **269**, 7435-8. (1994).
83. Modriansky, M., Murdza-Inglis, D. L., Patel, H. V., Freeman, K. B. & Garlid, K. D. Identification by site-directed mutagenesis of three arginines in uncoupling protein that are essential for nucleotide binding and inhibition. *J Biol Chem* **272**, 24759-62. (1997).
84. Arechaga, I., Ledesma, A. & Rial, E. The Mitochondrial Uncoupling Protein UCP1: A Gated Pore. *IUBMB Life* **52**, 165-173 (2001).
85. Echtay, K. S., Bienengraeber, M., Winkler, E. & Klingenberg, M. In the uncoupling protein (UCP-1) His-214 is involved in the regulation of purine nucleoside triphosphate but not diphosphate binding. *J Biol Chem* **273**, 24368-74. (1998).
86. Echtay, K. S., Bienengraeber, M. & Klingenberg, M. Mutagenesis of the uncoupling protein of brown adipose tissue. Neutralization Of E190 largely abolishes pH control of nucleotide binding. *Biochemistry* **36**, 8253-60. (1997).
87. Echtay, K. S., Winkler, E., Bienengraeber, M. & Klingenberg, M. Site-directed mutagenesis identifies residues in uncoupling protein (UCP1) involved in three different functions. *Biochemistry* **39**, 3311-7. (2000).
88. Bouillaud, F. et al. A sequence related to a DNA recognition element is essential for the inhibition by nucleotides of proton transport through the mitochondrial uncoupling protein. *Embo J* **13**, 1990-7. (1994).
89. Gonzalez-Barroso, M. M. et al. Deletion of amino acids 261-269 in the brown fat uncoupling protein converts the carrier into a pore. *Biochemistry* **36**, 10930-5. (1997).

90. Arechaga, I. et al. Cysteine residues are not essential for uncoupling protein function. *Biochem J* **296**, 693-700. (1993).
91. Bienengraeber, M., Echtay, K. S. & Klingenberg, M. H+ transport by uncoupling protein (UCP-1) is dependent on a histidine pair, absent in UCP-2 and UCP-3. *Biochemistry* **37**, 3-8. (1998).
92. Gonzalez-Barroso, M. M. et al. Activation of the uncoupling protein by fatty acids is modulated by mutations in the C-terminal region of the protein. *Eur J Biochem* **239**, 445-50. (1996).
93. Klingenberg, M., Echtay, K. S., Bienengraeber, M., Winkler, E. & Huang, S. G. Structure-function relationship in UCP1. *Int J Obes Relat Metab Disord* **23 Suppl 6**, S24-9. (1999).
94. Winkler, E., Wachter, E. & Klingenberg, M. Identification of the pH sensor for nucleotide binding in the uncoupling protein from brown adipose tissue. *Biochemistry* **36**, 148-55. (1997).
95. Gonzalez-Barroso, M. M., Fleury, C., Bouillaud, F., Nicholls, D. G. & Rial, E. The uncoupling protein UCP1 does not increase the proton conductance of the inner mitochondrial membrane by functioning as a fatty acid anion transporter. *J Biol Chem* **273**, 15528-32. (1998).
96. Kozak, U. C. et al. An upstream enhancer regulating brown-fat-specific expression of the mitochondrial uncoupling protein gene. *Mol Cell Biol* **14**, 59-67. (1994).
97. Sears, I. B., MacGinnitie, M. A., Kovacs, L. G. & Graves, R. A. Differentiation-dependent expression of the brown adipocyte uncoupling protein gene: regulation by peroxisome proliferator-activated receptor gamma. *Mol Cell Biol* **16**, 3410-9. (1996).
98. Silva, J. E. & Rabelo, R. Regulation of the uncoupling protein gene expression. *Eur J Endocrinol* **136**, 251-64. (1997).
99. Cassard-Doulcier, A. M. et al. In vitro interactions between nuclear proteins and uncoupling protein gene promoter reveal several putative transactivating factors including Ets1, retinoid X receptor, thyroid hormone receptor, and a CACCC box- binding protein. *J Biol Chem* **269**, 24335-42. (1994).
100. Casteilla, L. et al. Stable expression of functional mitochondrial uncoupling protein in Chinese hamster ovary cells. *Proc Natl Acad Sci U S A* **87**, 5124-8. (1990).
101. Klaus, S., Casteilla, L., Bouillaud, F., Raimbault, S. & Ricquier, D. Expression of the brown fat mitochondria uncoupling protein in Xenopus oocytes and important into mitochondrial membrane. *Biochem Biophys Res Commun* **167**, 784-9. (1990).

102. Romanos, M. A., Scorer, C. A. & Clare, J. J. Foreign gene expression in yeast: a review. *Yeast* **8**, 423-88 (1992).

103. Romanos MA, H. F., Comerford SA, Scorer CA. Production of a phosphorylated GST::HPV-6 E7 fusion protein using a yeast expression vector and glutathione S-transferase fusions. *Gene* **152**, 137-8 (1995).

104. Scorer CA, B. R., Clare JJ, Romanos MA. The intracellular production and secretion of HIV-1 envelope protein in the methylotrophic yeast Pichia pastoris. **136**, 111-9 (1993).

105. Scorer CA, C. J., McCombie WR, Romanos MA, Sreekrishna K. Rapid selection using G418 of high copy number transformants of Pichia pastoris for high-level foreign gene expression. *Biotechnology (N Y).* **12**, 181-4 (1994).

106. Beesley KM, F. M., Clarke BE, Beesley JE, Dopping-Hepenstal PJ, Clare JJ, Brown F, Romanos MA. Expression in yeast of amino-terminal peptide fusions to hepatitis B core antigen and their immunological properties. *Biotechnology (N Y).* **8**, 644-9 (1990).

107. Smith, R. A., Duncan, M. J. & Moir, D. T. Heterologous protein secretion from yeast. *Science* **229**, 1219-24 (1985).

108. Kaplan, R. S. & Pedersen, P. L. Determination of microgram quantities of protein in the presence of milligram levels of lipid with amido black 10B. *Anal Biochem* **150**, 97-104. (1985).

109. Jezek, P., Orosz, D. E. & Garlid, K. D. Reconstitution of the uncoupling protein of brown adipose tissue mitochondria. Demonstration of GDP-sensitive halide anion uniport. *J Biol Chem* **265**, 19296-302. (1990).

110. Urbankova, E., Hanak, P., Skobisova, E., Ruzicka, M. & Jezek, P. Substitutional mutations in the uncoupling protein-specific sequences of mitochondrial uncoupling protein UCP1 lead to the reduction of fatty acid-induced H^+ uniport. *The International Journal of Biochemistry & Cell Biology* **32**, 212-220 (2003).

111. Hanak, P. & Jezek, P. Mitochondrial uncoupling proteins and phylogenesis - UCP4 as the ancestral uncoupling protein. *FEBS Lett* **495**, 137-41. (2001).

112. Hagen, T. & Lowell, B. B. Chimeric proteins between UCP1 and UCP3: the middle third of UCP1 is necessary and sufficient for activation by fatty acids. *Biochem Biophys Res Commun* **276**, 642-8. (2000).

113. Klingenberg, M. & .

Uncoupling Proteins-How Do They Work and How Are They Regulated. *IUBMB Life* **52**, 175-179 (2001).

114. Garlid, K. D., Jaburek, M., Jezek, P. & Varecha, M. How do uncoupling proteins uncouple? *Biochim Biophys Acta* **1459**, 383-389. (2000).

115. Echtay, K. S., Winkler, E., Klingenberg, M. Coenzyme Q is an obligatory cofactor for uncoupling protein function. *Nature* **408**, 609-13. (2000)

11 Appendix